remote sensing

MDPI

Article

SEVIRI Aerosol Optical Depth Validation Using AERONET and Intercomparison with MODIS in Central and Eastern Europe

Ajtai Nicolae [1], Mereuta Alexandru [1,*], Stefanie Horatiu [1], Radovici Andrei [1], Botezan Camelia [1], Zawadzka-Manko Olga [2], Iwona S. Stachlewska [2], Stebel Kerstin [3] and Zehner Claus [4]

1 Faculty of Environmental Science and Engineering, Babeș-Bolyai University, 30 Fantanele St., 400294 Cluj-Napoca, Romania; nicolae.ajtai@ubbcluj.ro (A.N.); horatiu.stefanie@ubbcluj.ro (S.H.); andrei.radovici@ubbcluj.ro (R.A.); camelia.botezan@ubbcluj.ro (B.C.)
2 Faculty of Physics, University of Warsaw, Pasteura 5, 02-093 Warsaw, Poland; olga.zawadzka@fuw.edu.pl (Z.-M.O.); iwona.stachlewska@fuw.edu.pl (I.S.S.)
3 NILU—Norwegian Institute for Air Research NILU, Instituttveien 18, 2007 Kjeller, Norway; kst@nilu.no
4 European Space Research Institute, European Space Agency, 00044 Frascati, Italy; claus.zehner@esa.int
* Correspondence: alexandru.mereuta@ubbcluj.ro

Abstract: This paper presents the validation results of Aerosol Optical Depth (AOD) retrieved from the Spinning Enhanced Visible Infrared Radiometer (SEVIRI) data using the near-real-time algorithm further developed in the frame of the Satellite-based Monitoring Initiative for Regional Air quality (SAMIRA) project. The SEVIRI AOD was compared against multiple data sources: six stations of the Aerosol Robotic Network (AERONET) in Romania and Poland, three stations of the Aerosol Research Network in Poland (Poland–AOD) and Moderate Resolution Imaging Spectroradiometer (MODIS) data overlapping Romania, Czech Republic and Poland. The correlation values between a four-month dataset (June–September 2014) from SEVIRI and the closest temporally available data for both ground-based and satellite products were identified. The comparison of the SEVIRI AOD with the AERONET AOD observations generally shows a good correlation (r = 0.48–0.83). The mean bias is 0.10–0.14 and the root mean square error RMSE is between 0.11 and 0.15 for all six stations cases. For the comparison with Poland–AOD correlation values are 0.55 to 0.71. The mean bias is 0.04–0.13 and RMSE is between 0.10 and 0.14. As for the intercomparison to MODIS AOD, correlations values were generally lower (r = 0.33–0.39). Biases of −0.06 to 0.24 and RMSE of 0.04 to 0.28 were in good agreement with the ground–stations retrievals. The validation of SEVIRI AOD with AERONET results in the best correlations followed by the Poland–AOD network and MODIS retrievals. The average uncertainty estimates are evaluated resulting in most of the AOD values falling above the expected error range. A revised uncertainty estimate is proposed by including the observed bias form the AERONET validation efforts.

Keywords: SEVIRI; AERONET; MODIS; Aerosol Optical Depth; validation

Citation: Nicolae, A.; Alexandru, M.; Horatiu, S.; Andrei, R.; Camelia, B.; Olga, Z.-M.; Stachlewska, I.S.; Kerstin, S.; Claus, Z. SEVIRI Aerosol Optical Depth Validation Using AERONET and Intercomparison with MODIS in Central and Eastern Europe. *Remote Sens.* **2021**, *13*, 844. https://doi.org/10.3390/rs13050844

Academic Editor: Manuel Antón

Received: 13 January 2021
Accepted: 18 February 2021
Published: 24 February 2021

1. Introduction

It is widely known that small particles suspended in the atmosphere (aerosols) have profound effects on human health [1] and the physical environment. The aerosols' effects on the physical environment emerge as a result of their ability to both scatter and absorb incident solar radiation and modify cloud properties. Because the impact of aerosols on climate is an uncertain topic [2], aerosols are the subject of intensive research [3].

The aerosol optical properties can be measured directly using ground-based measurements or derived from remote sensing observations. While both in-situ and ground-based measurements of aerosol properties provide high precision data, their spatial coverage is limited [4]. To cover this shortcoming, satellite imagery provides continuous spatial and temporal products regarding aerosol properties being the best practical solution for

obtaining global aerosol properties. Nevertheless, the wide variety of sensors, retrieval algorithms, aerosol models and radiative transfer calculations, all contribute to higher uncertainty estimates as opposed to other retrieval methods and instruments [5,6]. Retrieval errors can be induced by sensor calibration issues [7]. Differences in aerosol optical models may induce retrieval uncertainties based on regional and seasonal aerosol trends [8].

The aerosol optical depth (AOD) is the vertical integral of the aerosol extinction coefficient from the earth surface to the top of the atmosphere [9], representing the relation between the aerosol loading and radiation. Over time, a series of methods for AOD retrieval over land have been developed for different detectors: Polar orbiting single view—Total Ozone Mapping Spectrometer - TOMS [10,11]; Advance Very-High Resolution Radiometer—AVHRR [12,13]; Sea-viewing Wide Field-of-view Sensor—SeaWiFS [14–16]; Moderate Resolution Imaging Spectroradiometer—MODIS [16–21]; Ozone Monitoring Instrument—OMI [22–25]; Visible Infrared Imaging Radiometer Suite—VIIRS [26,27]; Polarization and Directionality of the Earth's Reflectance—POLDER [28,29]; Atmospheric InfraRed Sounder—AIRS [30,31]; Infrared Atmospheric Sounder Interferometer—IASI [32]; MEdium Resolution Imaging Spectrometer—MERIS [33,34]; Ocean Land Colour Instrument—OLCI [35]; dual view: The Advanced Along Track Scanning Radiometer—AATSR [33,36,37]; Sea and Land Surface Temperature Radiometer—SLSTR [38,39]; multi angle: Multi-angle Imaging SpectroRadiometer—MISR [40–43]; limb view: SCanning Imaging Absorption SpectroMeter for Atmospheric CHartographY—SCIAMACHY [44,45]; OMPS [46,47]; Stratospheric Aerosol and Gas Experiment—SAGE [48]; Optical Spectrograph and InfraRed Imaging System—OSIRIS [49,50]; lidar: Cloud-Aerosol Lidar with Orthogonal Polarization (CALIOP) [51,52]; Geostationary—Geostationary Operational Environmental Satellite—GOES [53–55]; Spinning Enhanced Visible and Infrared Imager—SEVIRI [56–59]; The Advanced Himawari Imager—AHI [60–62]. A comprehensive list of satellite instruments used for column AOD retrieval and/or aerosol extinction profiles can be found in the scientific literature [63,64].

Satellite AOD related products, however, are characterized by high uncertainties in the retrieval of aerosol properties over land than ocean due to higher surface reflectance, as well as considerable temporal variability and spatial disturbances of this parameter [57]. Palacios-Peña et al., 2018 [65] evaluated the AOD representation of different satellite sensors, where MODIS AOD showed the best agreement with AERONET observations. When applying similar algorithm principles to similar sensors, significant differences can be expected in the datasets [13,17,26]. These differences increase when comparing products from different sensors and algorithms [66]. The approach to cloud masking is also a bias source when comparing datasets from similar retrieval algorithms [67,68].

The temporal resolution of data is determined by the satellite type: polar orbiting satellites have poor temporal resolution due to their long revisit time, while high temporal resolution is provided by geostationary satellites. The Meteosat Second Generation (MSG) geostationary satellites monitor Europe with the use of the Spinning Enhanced Visible and Infrared Imager (SEVIRI) instrument, measures radiance with a high time resolution (15 min) and a good spatial resolution of 3 km in nadir. SEVIRI-based AOD data product is validated in this paper. In order to improve the quality of the data concerning the aerosol properties retrieved by satellites, a comparison of the data provided by different instruments is generally conducted. Several studies [5,57,69–74] are focused on joint use of satellite and ground-based observations, mostly collected within the Aerosol Robotic Network—AERONET [75]. Intercomparison of satellite datasets may be challenging. In some cases, datasets may end up being mismatched by different retrieval resolutions, spatial, temporal and channel (wavelength dependent) inconsistencies [5,6]. However, a multi-sensor validation approach is essential for improving aerosol retrieval algorithms while also highlighting their limitations.

It is much more challenging to estimate AOD from geostationary satellite retrievals than it is to do so based on data acquired from low earth orbit satellites [76]. However, advances in retrieval algorithms for geostationary satellites are found in scientific literature,

with direct applications of SEVIRI data [29,56,57,59,77–82]. The main advantage in these approaches is the higher temporal resolution that the geostationary satellites provide, e.g., [58]. Other works focus on climate data records based on daily and monthly estimates of SEVIRI AOD over land and ocean surfaces [83].

Zawadzka and Markowicz 2014 [57], developed one- and two-channel algorithms for deriving AOD from a synergy of satellite and ground-based observations, using data from Poland measured between 2009 and 2011. They found a good correlation between the AOD data retrieved from SEVIRI and the sun photometer observations with bias values between 0.01–0.02 and root mean square error values of about 0.05 for both one- and two-channels methods. Their method was further developed within the SAMIRA project [84] into a near-real-time (NRT) AOD retrieval algorithm for the domain of Poland, Romania, Czech Republic and Southern Norway. Moving forward, we will use the term SEVIRI NRT to denote the NRT retrieval of AOD for SEVIRI irradiances at 531 nm. The algorithm is described in detail in [58].

The current paper deals with the validation of the SEVIRI NRT AOD data against ground-based measurements (AERONET and the Poland–AOD Network) which are inherently not affected by surface reflectance compared to satellite retrievals. The uncertainty estimate described in [58] is also evaluated in this paper. An intercomparison between SEVIRI and MODIS AOD is also performed to add to the robustness of the results.

The paper is structured as follows. In Section 2, data use and the methods proposed are described for both ground-based (AERONET and the Poland–AOD Network) validation and for the intercomparison between satellite retrievals (SEVIRI and MODIS). In Section 3, we discuss the validation and intercomparison results based on each individual approach. A revised uncertainty estimation is also discussed in this Section. Finally, the paper is summarized and concluded in Section 4.

2. Data and Methods

2.1. Data

This Section describes the data used in the validation and intercomparison of the SEVIRI AOD with data from two ground-based networks (AERONET and the Poland–AOD Network) and with MODIS data, respectively.

2.1.1. SEVIRI AOD Retrieval Algorithm and Data

The SEVIRI instrument on board Meteosat Second Generation 2 is monitoring aerosol loadings over land at high temporal and spatial resolutions [85]. The MSG2 is a geostationary satellite developed by the European Organization for the Exploitation of Meteorological Satellites (EUMETSAT) in collaboration with the European Space Agency (ESA). The SEVIRI instrument collects data in 12 spectral channels in the visible, near-infrared and thermal-infrared part of the spectrum (between 0.635 and 13.4 μm), although the AOD data analysed in this study is derived from radiance measurements conducted within channel 1 (635 nm). The visible Earth disk as seen by SEVIRI is contained in 3712 × 3712 single pixels, each pixel being roughly a 5 × 5 km; actual size of the pixel varies with geographical position [57]. The spatial resolution of AOD values from the NRT application used in validation is between 4.5 × 5 km and 5.5 × 5 km depending on geographical positioning, with a temporal resolution of 15 minutes.

Regarding the SEVIRI AOD retrieval algorithm [57], it is important to mention that the removing of cloud-contaminated pixels was the first step and was done in accordance with a method developed by [86]. The next step, specifically for the one channel retrieval, was to determine the surface reflectance for a reference clear day (τ_{ref}) using radiance and aerosol optical properties. The AOD on reference days is obtained from the Copernicus Atmospheric Monitoring Service (CAMS) AOD forecast product which is corrected using ground-based observation (AERONET and Poland–AOD Network) and the optimal interpolation method [87]. Note that, the AERONET and Poland–AOD network data are not used for correcting the SEVIRI-AOD, but for correcting the CAMS data. Moreover,

this is done for different days than those used for the AOD calculations. The next step requires a minimization function, of the difference between the look-up tables and SEVIRI measured reflectance, in order to estimate the surface reflectance. As a result, AOD values are retrieved for several days following the reference day [58].

The degree of uncertainty of the retrieved AOD is dependent on the specific conditions of a particular day: when the difference between a clear day (τ_{ref}) and a polluted day (τ_{ret}) is high, the uncertainty is low (2–9%), while in the other case, when the retrieval is done throughout a day with low AOD values (τ_{ret} = 0.2) the uncertainty varies from 4% to 23% [57]. A similar variation in the uncertainty of the retrieved AOD is manifested in accordance with the time of day: lower uncertainty for early morning (9–17%) and higher uncertainty for midday (12–35%). The SEVIRI NRT uncertainty estimations were achieved using a threshold approach which was less time consuming than analytic calculations. The total AOD uncertainty consisted of five components: surface reflectance estimates, AOD on the reference day, the AOD derived on the calculation day, cloud edges factor, and so-called "other sources" related to aerosol atmospheric parameters. Thus, the total SEVIRI AOD uncertainty amounts to ±10 % to ±40 % of the SEVIRI pixel level AOD. A detailed description of the SEVIRI AOD uncertainty estimation procedure can be found in [58].

2.1.2. Ground-Based Remote Sensing Data (AERONET and Poland–AOD)

The analysis was performed on data collected between 1 June and 30 September 2014. The SEVIRI AOD validation was done against six ground-based stations from AERONET and three stations from the Poland–AOD Network (Figure 1, the AERONET sites locations indicated as red squares and the Poland–AOD sites as blue triangles). The stations represent different orography (flatland, costal, mountains) and characteristics (urban, rural).

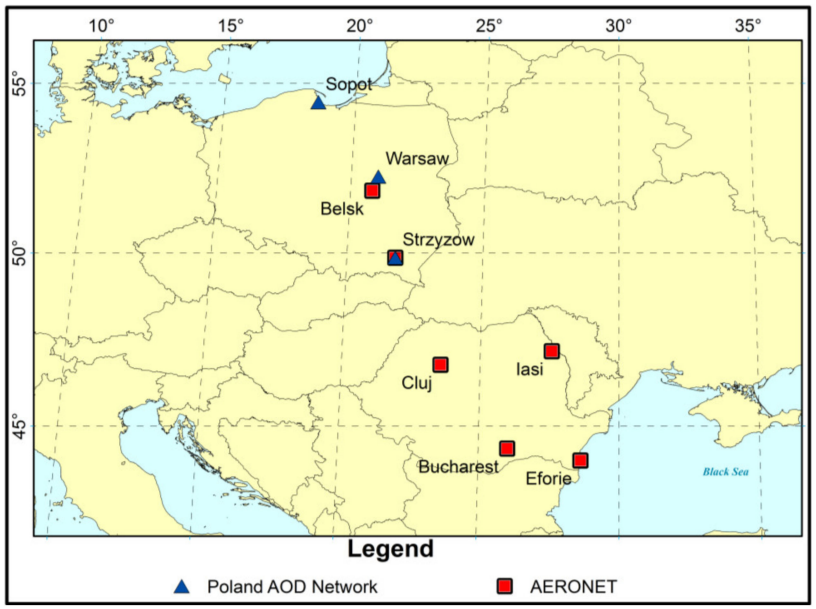

Figure 1. Ground stations used in the SEVIRI NRT AOD validation in the framework of SAMIRA.

Within the AERONET network, the measurements were made with the Cimel Electronique 318A sun photometers (675 nm) at four stations in Romania: Cluj, Iasi, Eforie and Bucharest and two in Poland: Belsk and Strzyzow. We used AERONET version 3 and AOD level 2 data, which was automatically cloud-cleared and manually inspected, with pre- and post-field calibration applied. Within the Poland–AOD Network, the measurements were made with the Multifilter Rotating Shadowband Radiometers MFR-7 radiometers (613 and 674 nm) at three stations: Warsaw, Sopot and Strzyzow.

2.1.3. MODIS Data

The Moderate Resolution Imaging Spectroradiometers (MODIS) onboard NASA's Terra and Aqua platforms have been retrieving aerosol parameters since 2000 and 2002, respectively [20]. The polar orbiting satellites perform daily overpasses at 10:30 and 13:30 local solar Equatorial crossing time [88]. The 3-km product offers several parameters, such as total AOD at 550 nm and fine mode fraction, based on the spectral fitting error. Detailed descriptions of the Dark Target retrieval algorithm are presented extensively in the literature [17,89–95]. The 3 × 3 km AOD product selected for this study provides the highest quality assurance confidence (QAC) for AOD at 550 nm, QAC = 3 over land and QAC > 1 over ocean surfaces [21,96]. The estimated uncertainty for 66% of retrievals over land fall within ±0.05 ± 0.20 AOD [21]. This product was chosen for validation purposes since SEVIRI AOD product offers similar spatial resolution of (roughly 5 × 5 km SEVIRI vs. 3 × 3 km MODIS) and retrieval wavelengths (635 nm SEVIRI vs. 550 nm MODIS).

2.2. Methods

In this section, we provide a description of the methods used for the validation and intercomparison of the SEVIRI-AOD against ground-based networks (AERONET and Poland–AOD) and MODIS data, respectively. This section also describes the spatial and temporal matching method between datasets and presents the uncertainties estimation approach.

2.2.1. Validation Methodology against Ground-Based Networks (AERONET and Poland–AOD)

The analysis was performed on data collected between 1 June and 30 September 2014. AERONET and Poland–AOD datasets were refined in order to allocate the closest in time columnar AOD value corresponding within 15 minutes to each SEVIRI measurement. The validation of the SEVIRI AOD data was done by comparing the overlapping pixel with the ground stations observations. The spatial collocation was done by matching the spatial coordinates of the AERONET stations to the centre coordinates of the nearest SEVIRI AOD pixel. Given that the SEVIRI AOD pixel resolution did not exceed 5.5 × 5 km, the distance between the pixel centre and the AERONET station could not exceed 3.72 km. In the case of AERONET stations collocated data was not available for each SEVIRI AOD measurement due to spatial and temporal mismatching. Regarding the Poland–AOD Network, corresponding measurements were available for most of the SEVIRI AOD data. The number of collocated data points on a single cloud-free day in a single location is at maximum of 19 and of 15, respectively, for the SEVIRI retrieval window in the morning (5:00–9:45 UTC) and afternoon (13:00–16:45 UTC). On average, clouds would affect 50% of the potentially available data points in summer and up to 80% in winter. Given the fact that ground-based measurements are considered reference for this study, a comparison was conducted between the data provided by the AERONET and Poland–AOD networks in order to determine the consistency of the data. This analysis was conducted for Strzyzow station where AOD values were available from both, the Cimel (675 nm) and the MFR 7 (674 nm) instruments. The AOD for both instruments was not converted to the same wavelength because the bias values are influenced in minor proportion by the different wavelengths at which data were collected (10^{-2} order of magnitude). Thresholds for the minimum values of the AOD derived from columnar ground-based measurements are commonly used, e.g., [97]. In this paper, an AOD value of 0.15 at 675 and 674 nm was used as a lower limit for comparisons.

In order to determine if the SEVERI uncertainties are correctly estimated, the delta values were calculated for each pair of measurements using the following formula:

$$\begin{aligned} \Delta &= (AOD_{SEVIRI} - AOD_{AERONET})/\text{sqrt}\,(\sigma^2{}_{SEVIRI} + \sigma^2{}_{AERONET} + \sigma^2{}_{RE}) \\ &\approx (AOD_{SEVIRI} - AOD_{AERONET})/\sigma_{SEVIRI} \end{aligned} \quad (1)$$

where AOD_{SEVIRI} is the SEVIRI pixel level AOD, $AOD_{AERONET}$ is the AOD retrieved from direct sun photometer measurements, σ_{SEVIRI} is the uncertainty of the AOD_{SEVIRI},

$\sigma_{AERONET}$ is the uncertainty of $AOD_{AERONET}$, and σ_{RE} is the uncertainty associated with the representativity error of the AERONET site. AERONET AOD is substantially more accurate than satellites products, therefore it is well justified to neglect the uncertainty in AERONET observations [98]. If, in addition, we disregard the possible issues with their ability to represent a satellite pixel area, the "error" in the retrieval can be approximated by the difference between the satellite and AERONET retrievals. Representativity errors are not accounted for in the SEVIRI AOD data product, therefore, for this simplistic uncertainty validation approach, we neglected them, even though they can be significant for some sites [99]. If Δ is normally distributed, 68.3 % of values should fall within the range $[-1, +1]$. If the fraction is smaller, then uncertainties are underestimated, if it is larger, then uncertainties are overestimated.

2.2.2. Intercomparison Method with MODIS Data

SEVIRI AOD retrievals data from 1 June and 30 September 2014 were selected for comparison with MODIS AOD data. The interval chosen for the intercomparison was constrained to this period considering the algorithm limitations such as low elevation angles and cloud cover during late autumn, winter and early spring conditions. The current data availability would not be sufficient to draw long-term climatological conclusions at this stage of development. The SEVIRI measurements windows in the morning (5:00–9:45 UTC) and in the afternoon (13:00–16:45 UTC) correspond to the Terra/MODIS (morning) and Aqua/MODIS (afternoon) measurements as follows: 8:30–10:30 UTC, Romania domain; 9:00–11:00 UTC, Poland and Czech Republic domain, for Terra; no retrieval matches within a one-hour window of the Aqua overpass (10:30–12:30). Hence, a temporal overlap can be achieved at maximum of twice per day (two matching datasets), since SEVIRI is a geostationary orbit, while Terra and Aqua are polar-orbiting satellites.

The availability of MODIS and SEVIRI data for a specific region does not always overlap. The differences are in the geometrical configuration of overpasses, their timing and spatial resolution. The given intervals of the SEVIRI measurements windows in the morning (5:00–9:45 UTC) and the afternoon (13:00–16:45 UTC) are strictly related to the limitations of the SEVIRI algorithm, that are discussed in detail in [57,58]. Mainly two of them are related to the given above retrieval windows: the low solar elevation angle (limiting observations during wintertime and in early morning and late evening) and the solar angle close to zenith (limiting observations around noon). The average area for each domain is described in detail by [58]. Spatial collocation was done using a closest-pixel approach where each SEVIRI AOD pixel was matched with the closest MODIS AOD pixel. If the dataset from Terra was retrieved within one hour or less of any of the SEVIRI datasets, the two closest datasets were matched. The SEVIRI temporal resolution is 15 minutes; however, due to algorithm constraints, not all the 15-minute slots were compared with the corresponding Terra or Aqua overpass. In cases where there was no exact matching timestamp, the two closest datasets were used, but in this case the difference in time was thresholded in order not to exceed one hour. In some cases, since the retrieval area from the MODIS granule did not always correspond to the entire surface domain of the selected country, it was necessary to use two MODIS granules, at 5 minutes time interval, overlapping the entire domain. Matching datasets from MODIS and SEVIRI may result in a low spatial overlap due to cloud cover variability. In cases were cloud screening resulted in less than 50% of SEVIRI total pixel count for any given domain area the matching datasets were discarded. A further selection criterion was applied specific to each domain based on daily SEVIRI total pixel count. Thus, to maintain a high statistical relevance, we selected matching datasets in which the number of collocated MODIS pixels represents at least 50% of the total number of SEVIRI AOD pixels, on any given day for any given domain. Following the recommended threshold for "clean" reference days, AOD values <0.15 were discarded [58]. Daily cases that satisfy the criteria were constructed from one SEVIRI dataset and one matching MODIS dataset, specific to each of the three domains.

In order to assess how SEVIRI uncertainties are estimated, the following equation for each pair of matching AOD pixels to MODIS was used:

$$\Upsilon = (AOD_{SEVIRI} - AOD_{MODIS})/sqrt\ (\sigma^2_{SEVIRI} + \sigma^2_{MODIS}), \quad (2)$$

where AOD_{SEVIRI} is the SEVIRI pixel level AOD, AOD_{MODIS} is the MODIS pixel level AOD, σ_{SEVIRI} is the uncertainty of the AOD_{SEVIRI} with values ranging from $\pm$0.1 AOD to $\pm$0.4 AOD depending on surface reflectance, AOD on reference day, AOD on calculation day, cloud edges and other sources [58] and σ_{MODIS} is the uncertainty of the AOD_{MODIS} with values ranging from $\pm$(0.05 + 0.20 AOD) [21]

3. Results and Discussion

3.1. SEVIRI AOD vs. Ground-Based Networks Validation

We validated the SEVIRI AOD against AERONET and Poland AOD ground-based AOD observations.

A preliminary analysis was conducted for Strzyzow station to compare the AOD values using both Cimel (675 nm) and MFR 7 (674 nm) instruments. The results presented in Table 1 show very good correlations between data provided by the two instruments with a low bias of 0.002 and RMSE of 0.01. Values are also in good agreement with those obtained by [100].

Table 1. Summary statistics: Poland–AOD vs. AERONET AOD.

Station	N	r	Bias	RMSE
Strzyzow	375	0.979	0.002	0.01

This shows that the same validation approach can be used for both ground-based AOD observations.

3.1.1. SEVIRI AOD vs. AERONET Network

The number of analysed pairs varies between 122 at Strzyzow and 295 at Bucharest for validating the AOD of SEVIRI against AERONET. These data, along with the average uncertainty and the correlation coefficient (r) are listed in Table 2 along with the mean bias (Bias) and the root mean square error (RMSE). When RMSE and mean bias have similar values, this can be an indication of the presence of systematic errors.

Table 2. Summary statistics: SEVIRI AOD (635 nm) vs. AERONET AOD (675 nm).

Station	N	SEVIRI Mean AOD	AERONET Mean AOD	SEVIRI Mean Uncertainty (%)	r	Bias	RMSE
Cluj	277	0.26	0.12	18.5	0.57	0.13	0.15
Iasi	261	0.25	0.13	20.7	0.61	0.13	0.15
Eforie	149	0.29	0.14	21.3	0.83	0.14	0.16
Bucharest	295	0.27	0.18	21.7	0.48	0.09	0.12
Belsk	167	0.26	0.16	17.7	0.69	0.10	0.11
Strzyzow	122	0.24	0.13	18.1	0.53	0.11	0.13

The correlation plots of the AERONET AOD measured at the Romania and Poland sites with the SEVIRI AOD pixel, for each site location, are plotted for the observation period of June–September 2014 in Figure 2.

For the Romanian AERONET AOD sites, the correlation coefficient (r) ranges between 0.48 at Bucharest and 0.83 at Eforie, with the mean bias of 0.09 and 0.14, respectively. Sites in Poland registered correlations ranging from 0.53 to 0.69 with a mean bias of 0.11 and 0.10 respectively. The different correlation values between the sites could be explained by the different reflectance values specific to the land cover and orography within the satellite pixel. Higher land cover homogeneity within a single SEVIRI pixel results in better surface

reflectance estimation. For example, the AERONET station in Cluj-Napoca is in an urban area; however, the collocated pixel overlaps a larger area which also includes forest and agricultural lands resulting in higher uncertainty of the surface reflectance estimation.

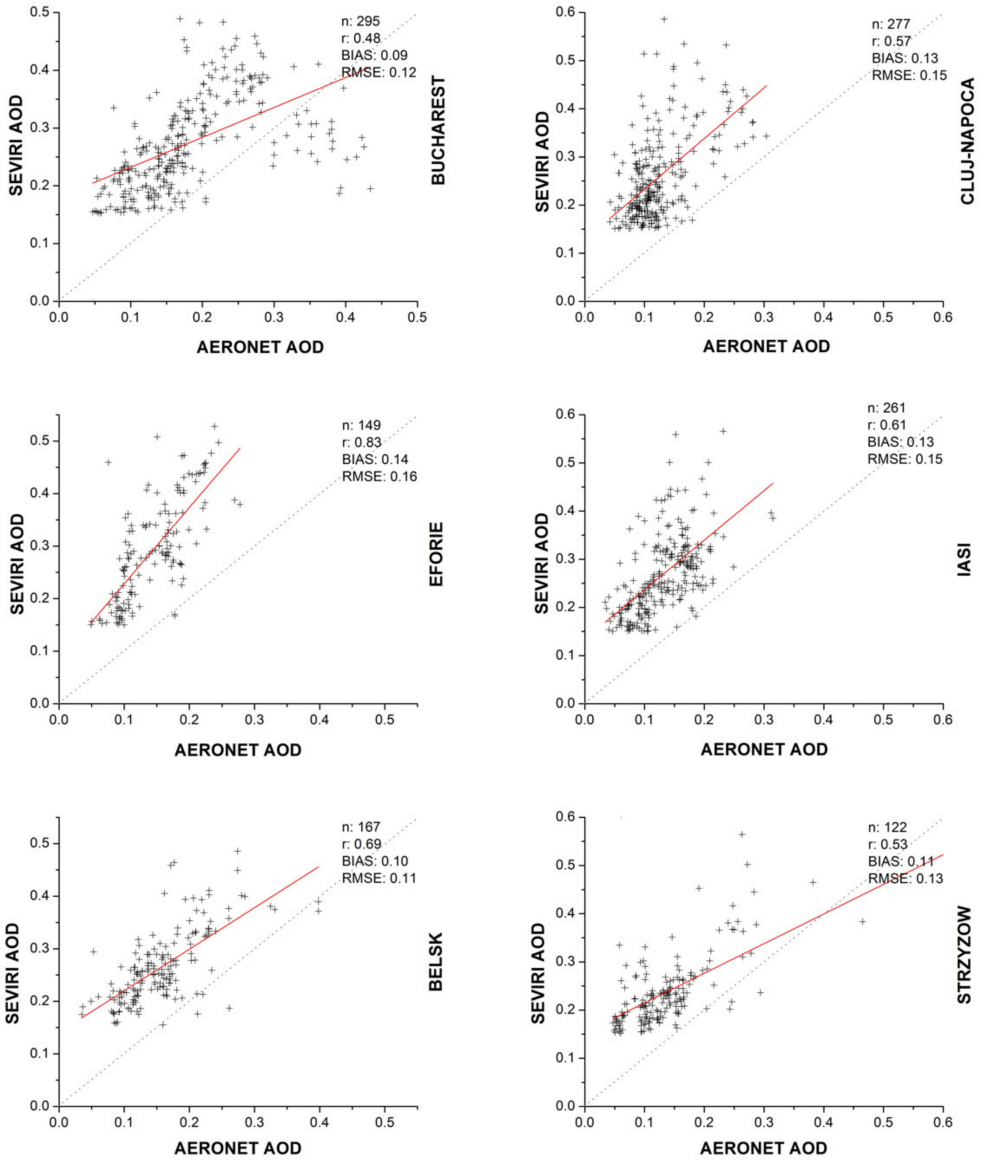

Figure 2. Correlation plots of the AOD (675 nm) measured in the Romanian AERONET sites in Bucharest, Cluj-Napoca, Eforie and Iasi, and Polish AERONET sites in Belsk and Strzyzow versus the SEVIRI AOD pixel (635 nm) derived for these locations during the period of June–September 2014. The red line shows linear fit.

3.1.2. SEVIRI AOD vs. Poland–AOD Network

A second analysis was conducted by comparing SEVIRI AOD to Poland–AOD ground-based measurements. The number of colocations ranged from 130 at Sopot to 238 at Warsaw. The main reason for the smaller number of collocations is that the Strzyzow station is located on a hilltop, therefore the results could be influenced by the orography, while Sopot is located very close to the Baltic coast being affected by unfavourable weather conditions such as a high frequency of cloud cover. The correlation coefficient (r) ranges between 0.57 at Sopot and 0.71 at Warsaw (613 nm). For the 674-nm channel, the correlations were slightly lower, 0.55 at Sopot to 0.68 at Warsaw, as listed in Table 3. The mean bias ranges

between 0.04 at 613 nm in Sopot and 0.13 at 674 nm in Warsaw. Correlation plots for the three Poland–AOD stations are seen in Figure 3.

Table 3. Summary statistics: SEVIRI AOD vs. a geostationary Poland–AOD.

Station	N	SEVIRI Mean AOD	Mean AOD 613 nm	Mean AOD 674 nm	r 613 nm	r 674 nm	Bias 613 nm	Bias 674 nm	RMSE 613 nm	RMSE 674 nm
Strzyzow	176	0.24	0.15	0.14	0.60	0.60	0.06	0.08	0.10	0.11
Warsaw	238	0.27	0.17	0.13	0.71	0.68	0.09	0.13	0.10	0.14
Sopot	130	0.26	0.18	0.15	0.57	0.55	0.04	0.07	0.11	0.13

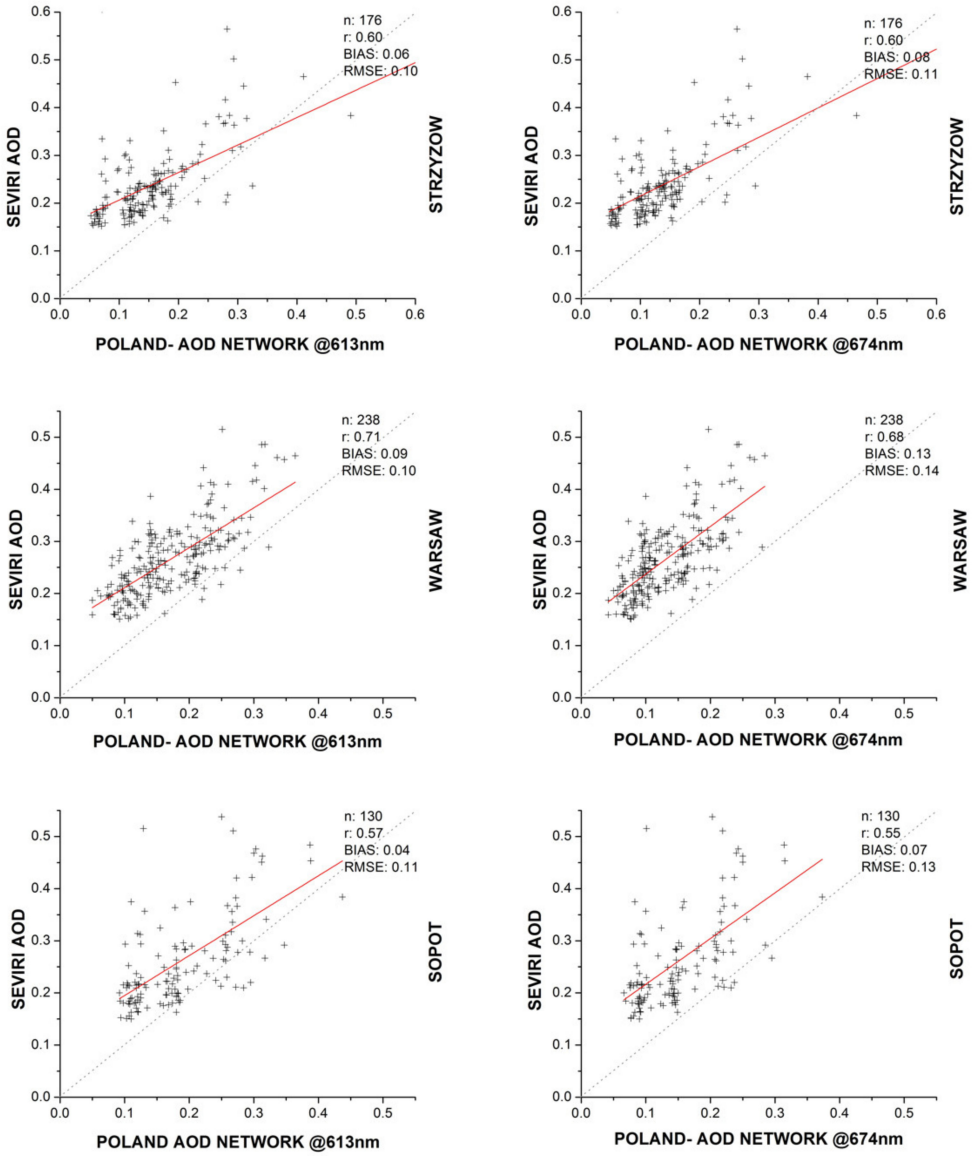

Figure 3. Correlation plots of the AOD measured in the Poland–AOD network sites in Warsaw Sopot and Strzyzow at 613 nm (**left**) and 674 nm (**right**) versus the SEVIRI AOD pixel (635 nm) derived for these locations during the period of June–September 2014. The red line shows linear fit.

3.1.3. SEVIRI AOD Uncertainties Validation

The number of Δ values within the [−1, +1] range (expected errors) for measurements at each station can be consulted in Table 4. Values for this interval ranged from 2.68 to

12.54 (%). The Δ distribution summarized for Poland and Romania is shown in Figure 4, considering the different thresholds of SEVIRI uncertainties. The values are randomly distributed, but generally above the [−1; +1] interval, an indication that the SEVIRI AOD uncertainties are underestimated.

Table 4. AOD uncertainties distribution (AERONET - 675 nm; POLAND–AOD - 674 nm).

Station	N	No. of Δ Values between [−1;+1]	Percentage (%)
AERONET			
Cluj	277	8	2.88
Eforie	149	4	2.68
Iasi	261	10	3.83
Bucharest	295	37	12.54
Strzyzow	122	5	4.09
Belsk	167	10	5.98
POLAND–AOD			
Strzyzow	176	8	4.54
Warsaw	238	8	3.36
Sopot	130	12	9.23

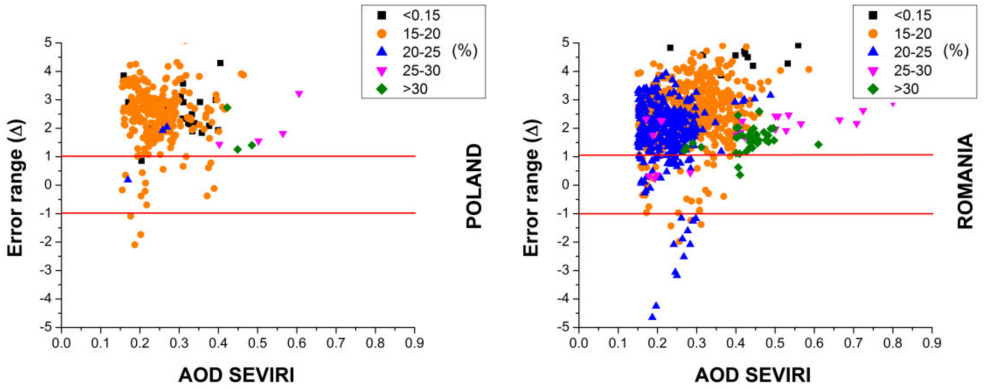

Figure 4. Expected error distribution versus SEVIRI AOD values for Poland (**left**) and Romania (**right**). Uncertainty thresholds, <15 to >30 (%) are represented by different coloured symbols.

3.2. SEVIRI NRT AOD vs. MODIS Level-2 AOD Intercomparison

From a maximum possible of 366 cases, the analysis was conducted on 35 cases, following our selection criteria, for Romania, Poland and Czech Republic. The comparable low number of co-located data is due to a multiple instances of high cloud coverage, spatial and temporal mismatching, and the lack of the SEVIRI data in August for the Czech Republic domain [58]. Table 5 shows the results representing the Romania domain. Correlation values ranged from −0.13 to 0.66 with 13 out of 19 cases resulting in average correlation between 0.33 and 0.66. We did not identify any obvious links between these values and pixel count nor the temporal differences. Mean bias values ranged from −0.01 to 0.18 with one outlier of 0.23. RMSE values ranged from 0.04 to 0.21 except on 14 September when it reached 0.26. In 6 of 19 cases more than 50% of AOD values fall within the expected error, while the remaining 13 cases fall above the interval. This is to be expected, as MODIS is known to underestimate instances of high AOD while overestimating lower values [19,21]. Another factor responsible for these values above the interval is the strong overestimation of AOD from the SEVIRI product, in particular for the Romanian domain, as seen in the SEVIRI-AERONET comparison from Section 3.1.1. Since low AOD values (<0.15) were discarded, all but one case showed an overestimation of SEVIRI AOD retrievals.

Table 5. Statistics: SEVIRI AOD vs. MODIS AOD—Romania.

Date	Δt (min)	Number of Pairs	Mean SEVIRI AOD	Mean MODIS AOD	r	Bias	RMSE	BELOW EE (%)	EE (%)	ABOVE EE (%)
14-August	50	8352	0.24	0.23	0.35	0.01	0.08	2.1	88.3	9.6
12-August	15	5078	0.31	0.34	0.66	−0.01	0.04	10.4	83.9	5.7
21-August	55	4775	0.24	0.22	0.45	0.01	0.08	1.8	84.8	13.4
23-June	45	1750	0.23	0.23	−0.13	0.01	0.11	7.3	78	14.7
3-August	55	7404	0.29	0.24	0.06	0.05	0.13	5.0	63.5	31.6
18-September	35	6237	0.22	0.13	0.28	0.09	0.12	0.2	51.5	48.3
1-August	60	6211	0.28	0.18	0.38	0.11	0.14	1.6	46.3	52.2
30-June	5	2858	0.22	0.13	0.44	0.08	0.12	1.6	46.5	51.9
2-September	50	3886	0.37	0.19	0.44	0.13	0.17	0.1	43.5	56.4
10-June	60	5572	0.31	0.18	−0.07	0.14	0.20	2.7	43.1	54.2
9-June	20	5220	0.30	0.19	−0.07	0.11	0.17	5.7	41.7	52.6
8-September	0	3672	0.33	0.18	0.50	0.15	0.18	0.1	31.6	68.4
30-August	5	4227	0.26	0.12	0.52	0.14	0.16	0	26.9	73.1
9-September	40	6833	0.37	0.19	0.36	0.18	0.21	0.8	30.7	68.5
11-September	15	6214	0.38	0.20	0.36	0.18	0.21	0.1	27.7	72.3
27-August	0	2950	0.31	0.15	0.38	0.16	0.19	0.1	28.4	71.5
6-September	5	2811	0.26	0.12	0.48	0.17	0.20	4.3	27.2	68.5
2-July	40	3323	0.27	0.11	0.22	0.16	0.18	0.2	21.3	78.5
14-September	60	3367	0.44	0.21	0.63	0.23	0.26	0	12	88

Table 6 shows eight cases analysed for the Czech Republic domain. Like Romania, the results show no obvious correlations linked to the number of AOD pairs or the average temporal differences between SEVIRI and MODIS datasets (**Δt**). Since this domain was smaller, the number of successful pixel matches was also lower as opposed to the other domains. Apart from the case of 8 June, correlations ranged between 0.29 and 0.58. Apart from 11 June averaging higher RMSE and bias values, the remaining cases showed bias values of −0.06 to 0.13 and RMSE values up to 0.19. In 4 out of 8 cases, more than 50% of AOD values fell within the expected error range while the remaining 4 cases showed values above this range.

The low number of cases, 8, for the Poland domain was mainly due to cloud coverage. Judging by the values in Table 7, a similar overestimation of SEVIRI AOD values can be identified. Six out of eight cases showed correlations of 0.22 to 0.72, while the remaining two showed negative values. Like the Czech Republic, four out of eight cases showed more than 59% of AOD values within the expected error range while in the four remaining cases more than 50 % of values fell above the range. RMSE values ranged from 0.09 to 0.21 and bias values ranged from 0.02 to 0.19.

Visual representations of the AOD differences (SEVIRI-MODIS) were constructed to better assess their spatial distribution. Figure 5 shows these differences represented for the Romania domain, while Figure 6 presents the differences form the Poland and Czech Republic domains. RGB images were also used to identify the presence of clouds and thin cirrus formations which may have contaminated the AOD retrievals.

Table 6. Statistics: SEVIRI AOD vs. MODIS AOD—Czech Republic.

Date	Δt (min)	Number of Pairs	Mean SEVIRI AOD	Mean MODIS AOD	r	Bias	RMSE	BELOW EE (%)	EE (%)	ABOVE EE (%)
7-July	5	1325	0.27	0.25	0.58	0.02	0.09	1.3	87.6	11.1
17-September	60	1683	0.29	0.29	0.36	−0.006	0.11	10.9	79.1	9.9
5-September	35	2147	0.25	0.32	0.41	−0.06	0.11	23.8	73.6	2.6
19-July	5	1596	0.40	0.31	0.41	0.09	0.17	4.2	60.5	35.3
20-July	35	1955	0.33	0.19	0.34	0.13	0.19	0.4	43.5	56.1
10-June	0	2781	0.31	0.18	0.29	0.13	0.16	0.3	39.4	60.3
8-June	5	3169	0.26	0.17	0.02	0.09	0.13	1.7	39.4	58.8
11-June	60	1498	0.46	0.22	0.4	0.24	0.28	0.3	19.6	80.1

Table 7. Statistics: SEVIRI AOD vs. MODIS AOD—Poland.

Date	Δt (min)	Number of Pairs	Mean SEVIRI AOD	Mean MODIS AOD	r	Bias	RMSE	BELOW EE (%)	EE (%)	ABOVE EE (%)
7-September	35	4993	0.37	0.34	0.72	0.03	0.09	1.1	86.1	12.8
9-July	45	4157	0.28	0.23	0.42	0.05	0.08	1.9	77.8	20.3
8-June	5	8496	0.26	0.21	0.22	0.05	0.1	3.1	65.4	31.5
2-August	0	3475	0.37	0.35	−0.14	0.02	0.16	17.5	59.2	23.4
3-August	45	3280	0.35	0.23	−0.06	0.12	0.18	3.9	45.7	50.4
16-September	30	5215	0.41	0.26	0.71	0.15	0.18	0.3	42.1	57.7
18-September	20	9429	0.32	0.18	0.6	0.14	0.16	0	36.7	63.3
17-September	30	9867	0.39	0.20	0.67	0.19	0.21	0.1	19.8	80.1

In some cases, MODIS and SEVIRI AOD values can be influenced by the presence of sub-visible cirrus that can escape the algorithm's cirrus mask [101–104]. Other cloud contamination source arises in the presence of bright subpixel clouds [105]. Instances of thin cirrus contamination were identified on 23 June; 3, 12 and 14 August, resulting in local overestimations of MODIS AOD values (Figure 5, blue pixels). However, in most cases we identified an overestimation of SEVIRI values. This was especially true in regions of Romania with higher surface reflectance such as croplands in the East and West as opposed to darker vegetation in the Central and through the Carpathian regions. This is to be expected as for darker surface it is easier to estimate AOD, than for bright ones, since dark targets have a smaller contribution to the signal received by the sensor. For days with low AOD, 0.15–0.20 (according to MODIS), the largest differences in the regions were obtained. This difference may also be the result of higher AOD reference values used in SEVIRI retrievals for the corresponding reference days. In the case of 1 August and 14 September, differences within other regions may be attributed to a larger temporal offset and the presence of subpixel clouds.

For the Poland domain, the case on 2 August is an example of cirrus and cloud edge contamination in the MODIS retrievals thus resulting in negative differences. Cases from 16, 17 and 18 September may have been influenced by cirrus contamination in both MODIS and SEVIRI retrievals. The larger differences corresponded to Western regions where sub-visible cirrus clouds were present and the central region where MODIS retrieved low AOD values. Despite some areas with significant differences in these three consecutive days there were good correlations between the two methods (0.60–0.71). The Czech Republic domain was also affected by cirrus and subpixel cloud contamination on 5 and 17 September resulting in negative differences. In the remaining cases, there were no obvious reasons to describe the random distribution of biases. One important factor contributing to low correlations was the lack of ground-based measurements in Czech Republic. These datasets are used in the optimal interpolation method for estimating surface reflectance.

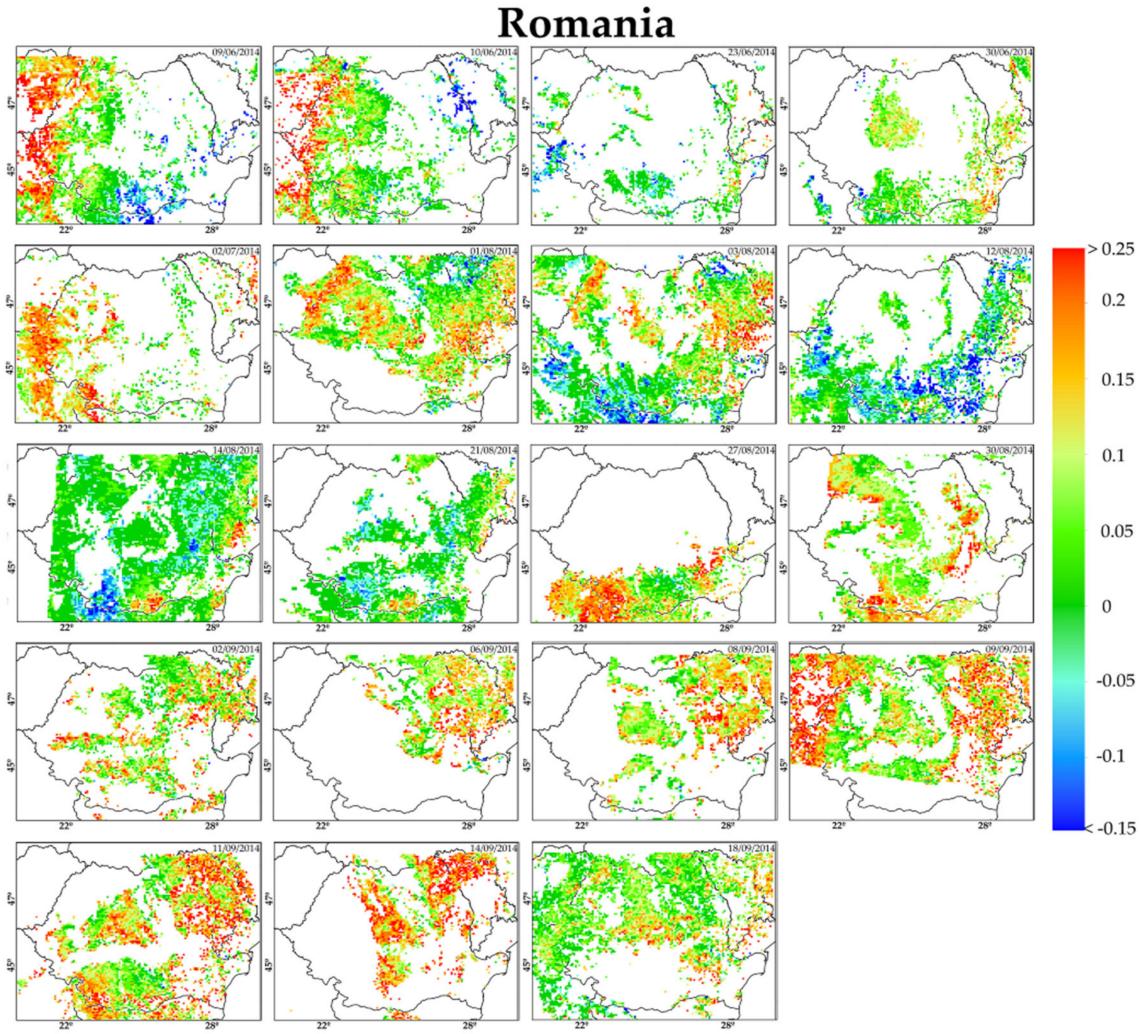

Figure 5. AOD differences between SEVIRI and MODIS for the Romania domain.

By comparing Figures 5 and 7, one can identify some instances of large differences that resulted from cloud edge contaminated pixels and are evident in Figure 7 where SEVIRI uncertainty values are much higher. Other areas with higher uncertainty values represent parts of Romania where surface reflectance estimates are higher (croplands). In cases of negative differences (MODIS cirrus contaminated pixels) SEVIRI uncertainties are also generally higher, between 20% and 30%. It seems that for days, with low cloud coverage, such as 9 and 11 September, uncertainties are less than 15% in the matching areas with higher differences. This may be a result of overestimations of surface reflectance.

Higher uncertainty values are generally seen for Poland and the Czech Republic in instances with cloud edge contamination, as seen in Figure 8. While in the case of the Czech Republic higher differences were in general agreement to higher uncertainty estimations, for Poland this was not always the case. For the cases of 16, 17 and 18 September, lower uncertainty values were seen over areas covered by thin cirrus. Larger differences were identified in regions with clear skies and moderate uncertain values, 15–20%. It is unclear at this point as to what caused these large differences, over 0.2 AOD. However, since these events were observed over three consecutive days, we may assume that higher AOD values from one reference day may have been a contributing factor.

The statistical distributions of SEVIRI AOD, MODIS AOD and AOD differences specific to each domain can be seen in Figure 9.

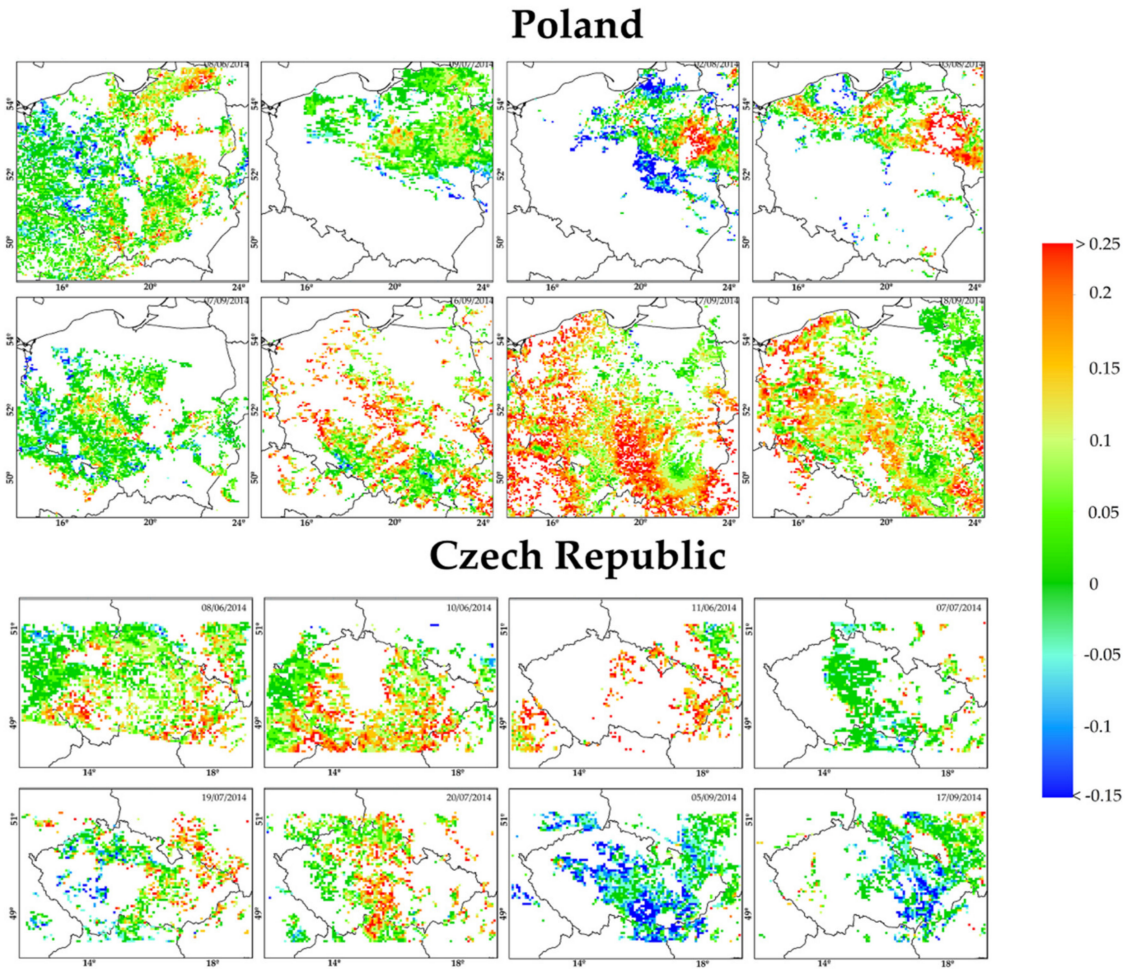

Figure 6. AOD differences between SEVIRI and MODIS for the Poland and Czech Republic domain.

Mean SEVIRI AOD values ranged from 0.30 to 0.34, while MODIS AOD values ranged from 0.18 to 0.23. AOD distributions from both sensors are positively skewed with SEVIRI skewness values ranging from 0.63 to 1.32, while MODIS skewness values ranged from 0.52 to 0.74. Regarding AOD differences (SEVIRI-MODIS) we obtained a near Gaussian shape for all three domains with average bias values of 0.08 for the Czech Republic and 0.10 for Poland and Romania. It should be noted that these bias values were also influenced by the decision to exclude low AOD (<0.15) from the statistical analysis. This factor increased the average bias by 0.03 (Romania) to 0.05 (Poland and the Czech Republic). Standard deviation values were also high ranging from 0.12 (Poland and Romania) to 0.14 (Czech Republic). This fact may in part be attributed to the low number of cases and subsequent AOD differences. RMSE also averaged high values 0.14 for Poland and 0.15 for the Czech Republic and Romania domains. In most cases, the largest differences were identified in areas with low AOD according to MODIS and moderate AOD according to SEVIRI. One factor influencing SEVIRI bias was the use of different wavelengths in the AOD retrievals, 550 nm by MODIS and 635 nm by SEVIRI. However, this bias is larger if we account for the spectral shift of AOD magnitude given by the Angström exponent. For the given time period and the selected domains, the average value of the Angström exponent (440/675 nm) was 1.59. This would relate to an increase in the bias by 0.04 for the Czech Republic and 0.05 for the Poland and Romania domain. It should be mentioned that the MODIS 3 km product is less robust than its 10 km counterpart and may exhibit higher uncertainties for low AOD situations [19,21]. Compared to the AERONET statistics from Poland and Romania, the high bias and RMSE values generated by SEVIRI versus MODIS seem to be in good agreement. However, the AERONET data sets account for a much lower number

of AOD retrievals the trend in bias and RMSE values was very similar. The same bias trend was identified compared to the Poland–AOD network; however, bias values were slightly lower. The latest validation efforts for the MODIS 3 km AOD product [19], for the European region, suggest good correlations with AERONET, mean r of 0.79, mean bias and RMSE of 0.043 and 0.11 respectively. However, biases are slightly larger for the MODIS Terra sensor. Compared to the SEVIRI-AERONET validations discussed in this paper the values seem to be in better agreement considering the relatively low number of collocations. In the cases of MODIS comparison, overestimation of SEVIRI values may also be attributed to factors such as surface reflectance estimates, different cloud masking techniques, spatial and temporal inconsistencies, retrieval geometry and the limited amount of statistical data.

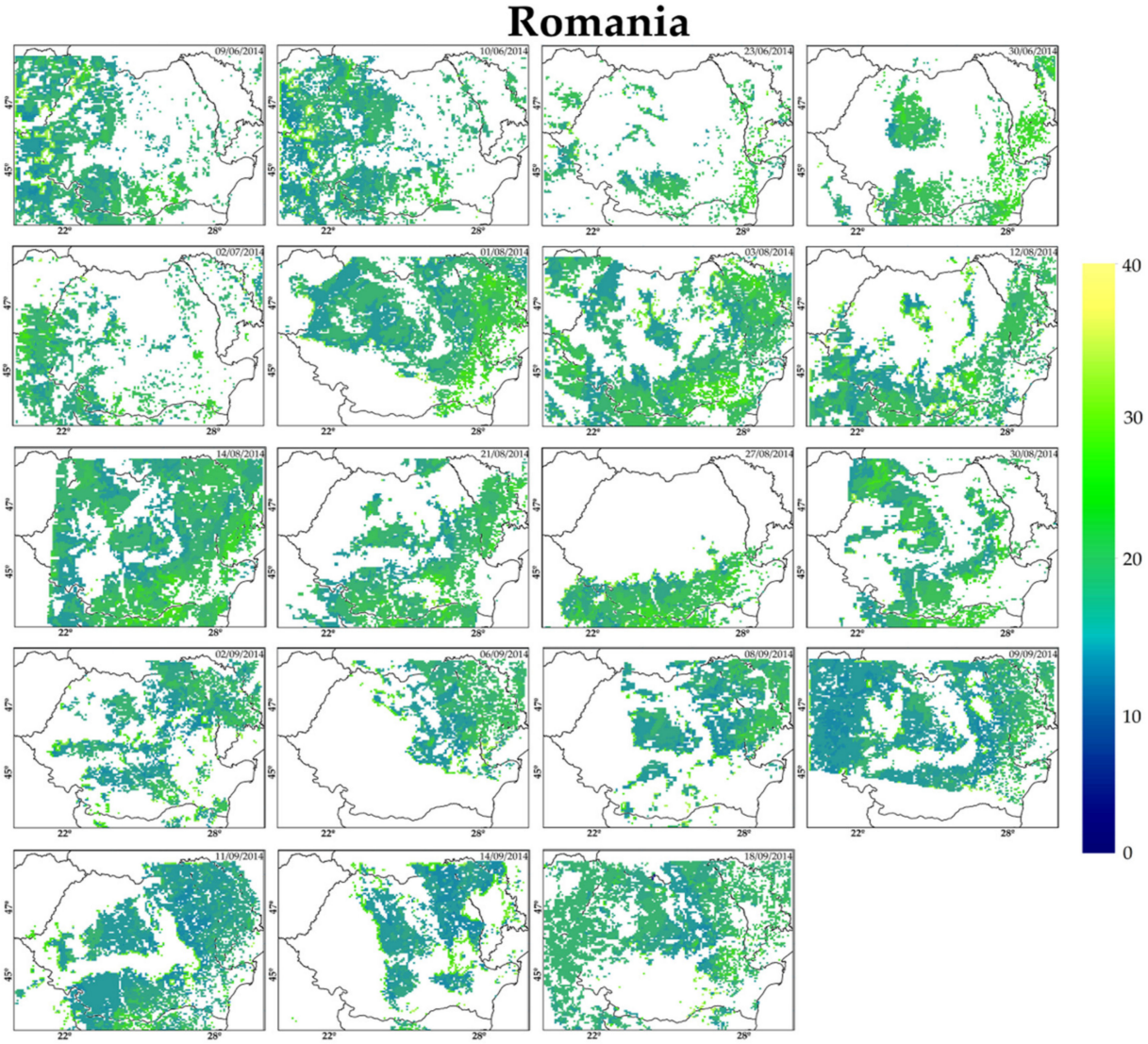

Figure 7. SEVIRI AOD uncertainty (UNC in %) specific for the Romanian domain.

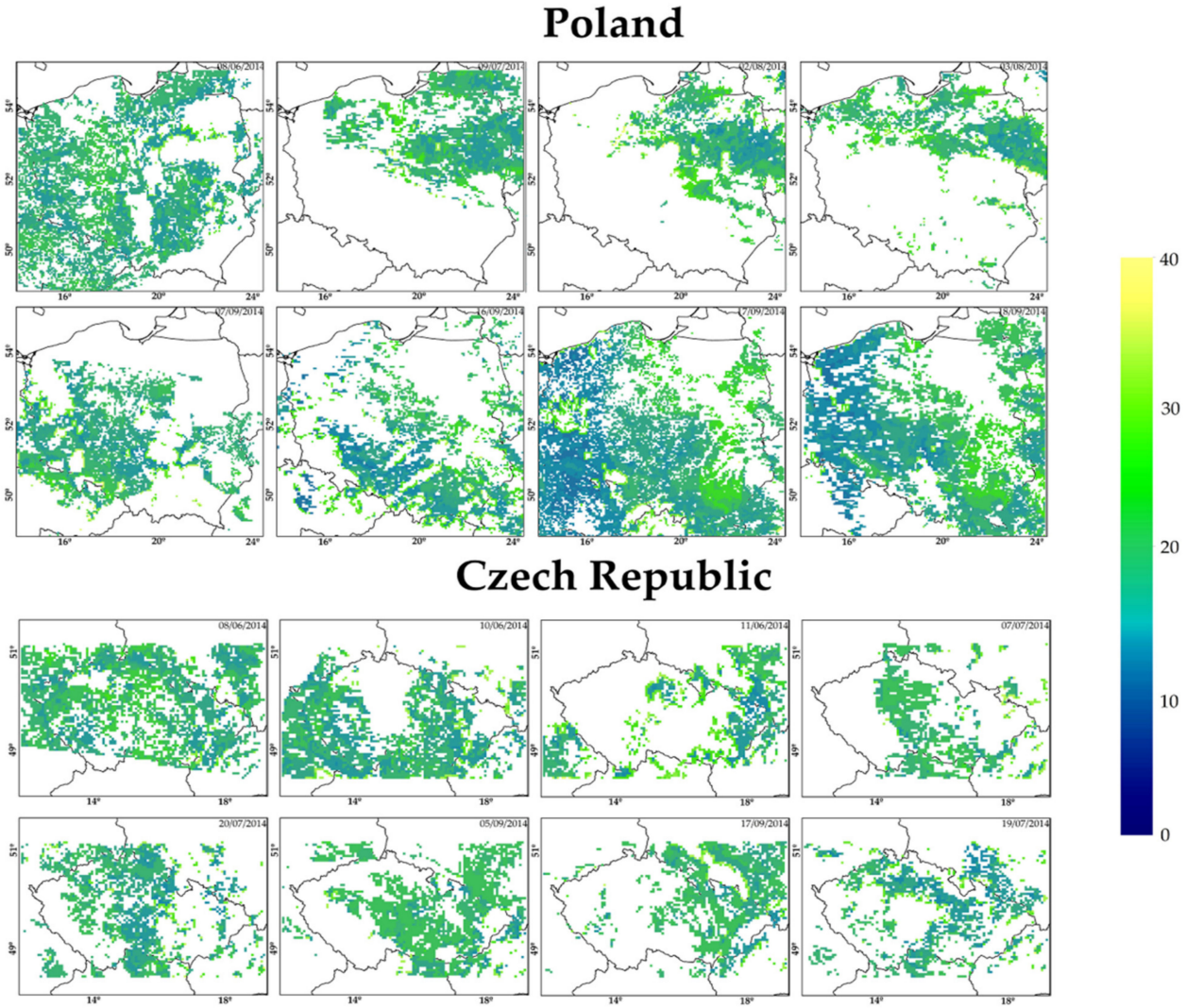

Figure 8. SEVIRI AOD uncertainty (UNC in %) specific for the Poland (upper) and Czech Republic (lower) domains.

3.3. Discussion on the Error Estimates for the SEVIRI NRT AOD

The estimated error of the SEVIRI NRT product was described in [58] and it addresses the random error that was estimated to be 10% to 40% of AOD. The AERONET validations in Section 3.1.1 indicate a strong overestimation of SEVIRI NRT AOD, also evident from the Poland–AOD comparison in Section 3.1.2. This bias representing systematic errors results in most of the Δ values falling above the [−1,+1] interval, as shown in Figure 5. The comparison with MODIS AOD, in Section 3.2., shows a better distribution of AOD values; however, the expected error range is not as stringent as in the case of AERONET and Poland–AOD.

Based on the bias values obtained in Section 3.1.1 we adjusted the SEVIRI estimate error accordingly: 0.12 + (±10 to ±40 % of AOD), where 0.12 represents the mean bias value according to the AERONET validation of the SEVIRI NRT AOD applications. The results of the uncertainty evaluation are presented in Table 8.

When correcting the estimate error, we can see that a significant number of AOD values fall within the error range. For the evaluation of SEVIRI AOD against AERONET, between 75.8% (Cluj-Napoca) and 94.6% (Bucharest) of AOD values satisfy the error range. For Poland–AOD, between 81.1% (Warsaw) and 94.5% (Strzyzow) of AOD values fall within the range. For the comparison with MODIS AOD, between 79.8% (Romania) and 83.8% (Czech Republic) of values fit the range criteria. Judging by these results, the

uncertainty range described by [58] could benefit from a bias adjustment. For a better estimation of the overall bias the validation efforts would also require a sensitivity test to different spatial and temporal averaging windows [21]. The limited time interval chosen for the study, 1 June–30 September 2014, could not account for seasonal differences. Thus, a further expansion of the SEVIRI NRT datasets would be beneficial for the evaluation of systematic errors and overall uncertainty estimations.

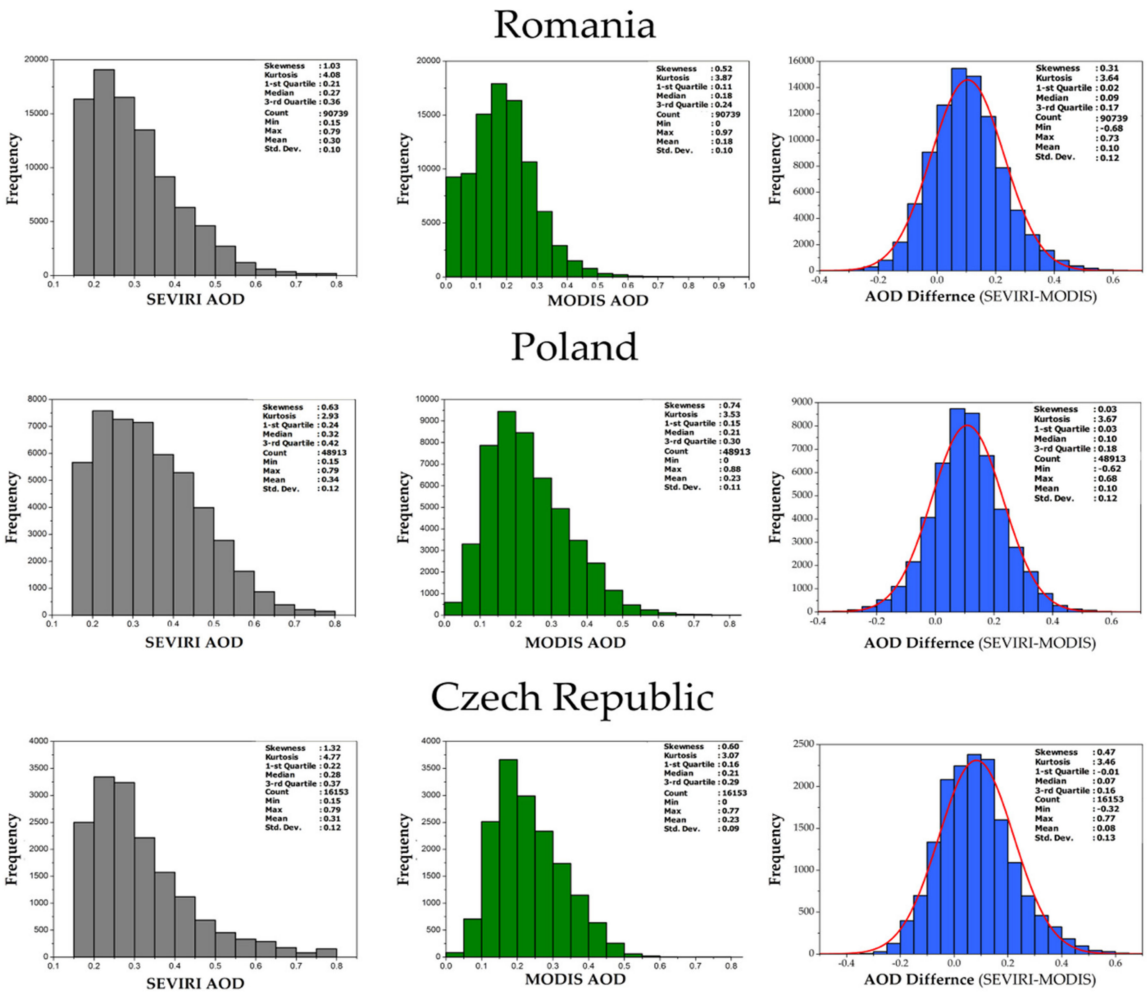

Figure 9. Distribution of SEVIRI AOD (left), MODIS AOD (centre) and AOD differences between SEVIRI and MODIS for Romania, Poland and Czech Republic.

Table 8. Comparison between the SEVIRI NRT AOD estimated error [58] and the bias-corrected estimated error.

Location	Estimated Error ±10 to ±40 % of AOD			Bias Corrected Estimated Error 0.12 + (±10 to ±40 % of AOD)		
	BELOW EE (%)	EE (%)	ABOVE EE (%)	BELOW EE (%)	EE (%)	ABOVE EE (%)
			AERONET			
Cluj	0.0	2.9	96.8	0.0	75.8	23.8
Eforie	0.0	2.7	97.3	0.0	80.5	19.5
Iasi	0.0	3.8	96.2	0.0	81.2	18.8
Bucharest	5.8	12.5	81.7	1.0	94.6	4.4
Strzyzow	0.8	4.1	95.1	0.0	90.2	9.8
Belsk	1.2	6.0	92.8	0.0	94.0	6.0

Table 8. *Cont.*

Location	Estimated Error ±10 to ±40 % of AOD			Bias Corrected Estimated Error 0.12 + (±10 to ±40 % of AOD)		
	BELOW EE (%)	EE (%)	ABOVE EE (%)	BELOW EE (%)	EE (%)	ABOVE EE (%)
			Poland–AOD			
Strzyzow	2.3	4.5	93.2	0.6	91.5	8.0
Warsaw	0.0	3.4	96.2	0.0	81.1	18.5
Sopot	0.0	9.2	90.8	0.0	90.0	10.0
			SEVIRI vs. MODIS			
Romania	2.1	48.4	49.6	0.4	79.8	19.9
Poland	2.4	49.6	48.0	0.6	80.5	18.9
Czech Republic	5.0	54.8	40.2	0.6	83.4	16.0

4. Conclusions

The study presents the validation of the SEVIRI NRT AOD product developed in the framework of the SAMIRA project. The AOD data sets were compared against three different instruments, AERONET, Poland–AOD network and MODIS over three domain areas corresponding to Romania, Poland and the Czech Republic. The validation efforts were conducted for a four-month period spanning from June to September 2014. Comparing SEVIRI AOD with AERONET AOD results in the best correlations followed by Poland–AOD network and MODIS retrievals. The AERONET data suggested good correlations (r) ranging from 0.48 to 0.83 representing the four stations in Romania (Cluj-Napoca, Iasi, Eforie and Bucharest) and 0.53 to 0.69 from two stations in Poland (Belsk and Strzyzow). AOD values where overestimated by SEVIRI retrievals registering a bias of 0.09–0.014 for the sites in Romania and 0.10–0.11 for sites in Poland. Correlations between POLAND–AOD and SEVIRI range from 0.55 to 0.71 on three separate locations (Strzyzow, Warsaw and Sopot) with biases ranging from 0.04 to 0.13. RMSE values were in good agreement, 0.11 to 0.15 for AERONET and 0.10 to 0.14 for Poland–AOD network. MODIS AOD values did not correlate as well with average r values of 0.33 for Romania, 0.35 for the Czech Republic and 0.39 for Poland. However, average biases ranging from 0.08 to 0.1 and RMSE of 0.12 to 0.14 were in good agreement to the ground–stations retrievals.

On average, MODIS AOD values were larger when contaminated by cirrus and cloud edges or sub-pixel clouds. As for SEVIRI retrievals, consistent biases were identified over areas with higher surface reflectance such as croplands. Higher uncertainty estimations seemed to correlate well with high AOD differences in case of cloud contaminated pixels. However, this was not the case for cropland areas. Significant AOD differences may also be attributed to spatial and temporal inconsistencies when matching satellite datasets. For ground-based retrievals, the overestimation of SEVIRI AOD values can be attributed to a multitude of factors such as wavelength inconsistencies, the limited amount of statistical data, surface reflectance estimations and orography. The uncertainty evaluation for the ground-based measurements shows that most values fall above the error range since SEVIRI AOD values are overestimated. When comparing SEVIRI NRT AOD to MODIS AOD, more values fall within the interval since this expected error range is larger. Based on the average bias collected form the AEROENT validation, a correction to the random estimated error was proposed. When applying this correction to the uncertainty evaluation we obtained the following uncertainty estimate: 0.12 + (±10 to ±40 % of AOD). The difference is significant for both ground-based and satellite comparisons. For the evaluation against the ground-based measurements, between 75.8% and 94.6% of AOD values satisfy the revised interval. The comparison between SEVIRI AOD and MODIS AOD shows between 79.8% (Romania) and 83.8% (Czech Republic) of values that fit the new interval. Further work is needed to

evaluate this bias when seasonal differences and different temporal and spatial collocation criteria are considered.

In the framework of the SAMIRA project, the SEVIRI NRT AOD product was further used as input data in order to derive near-surface hourly $PM_{2.5}$ maps for the study areas. Alongside the SEVIRI NRT AOD, WRF-CHEM model outputted aerosol species for the domain areas have been grouped in order to reconstruct the aerosol components defined in Global Aerosol Data Set (GADS) [106]. Mishchenko T-Matrix Inversion computation was applied to calculate the mass-to-extinction conversion factors for a wide range of aerosol classes in various humidity conditions and mass proportions. The data obtained from the T-matrix Inversion code were saved in the form of a Look-up Table (LUT). The Mishchenko code was run on 360.000 mixing ratios for the different species of aerosols that contribute to $PM_{2.5}$. Finally, the mass-to-extinction conversion factor from the LUT's was used to derive $PM_{2.5}$ from the SEVIRI NRT AOD data. An extended overview on the role of the SEVIRI AOD product in the SAMIRA project can be found in [84].

Author Contributions: Conceptualization, A.N., M.A., Z.-M.O. and I.S.S.; Formal analysis, M.A., R.A. and S.H.; Funding acquisition, A.N., S.K. and Z.C.; Investigation, A.N., M.A. and R.A. Methodology, A.N., M.A., S.H., B.C., I.S.S. and S.K.; Project administration, A.N., S.K.; Supervision, A.N., Z.-M.O. and I.S.S.; Validation, M.A., Z.-M.O. and S.K.; Visualization, R.A.; Writing—original draft, A.N., M.A. and S.H.; Writing—review & editing, A.N., M.A., S.H., B.C., Z.-M.O., I.S.S., S.K. and Z.C. All authors have read and agreed to the published version of the manuscript.

Funding: The research for this paper was financially supported by the ESA-ESRIN contract no. 4000117393/16/I-NB—Satellite-based Monitoring Initiative for Regional Air quality—SAMIRA. This work was supported by the Project entitled "*Development of ACTRIS-UBB infrastructure with the aim of contributing to pan-European research on atmospheric composition and climate change*" SMIS CODE 126436, co-financed by the European Union through the Competitiveness Operational Programme 2014–2020.

Institutional Review Board Statement: Not applicable.

Informed Consent Statement: Not applicable.

Data Availability Statement: AERONET Data is available in a publicly accessible repository that does not issue DOIs. Publicly available datasets were analyzed in this study. This data can be found here: https://aeronet.gsfc.nasa.gov/. The MODIS 3 km aerosol product data is available in a publicly accessible repository. The MODIS 3 km aerosol product data presented in this study are openly available in [MOD04_3K] at [DOI: 10.5067/MODIS/MOD04_3K.061]. SEVIRI NRT AOD data was obtained from the SAMIRA project and are available from University of Warsaw with the permission of Iwona Stachlewska (iwona.stachlewska@fuw.edu.pl). Poland-AOD data was obtained from the Poland-AOD network and are available with the permission of the PIs at: http://www.polandaod.pl/.

Acknowledgments: We thank the PIs and their teams for the effort in establishing and maintaining the following AERONET sites: Bucharest_INOE—Doina Nicolae, Cluj_UBB—Nicolae Ajtai, Eforie—Sabina Stefan, Iasi_LOASL—Marius Cazacu, Silviu Gurlui, Strzyzow—Krzysztof Markowicz, Belsk—Piotr Sobolewski, Brent Holben, Aleksander Pietruczuk. We thank the PIs and their teams for the effort in establishing and maintaining the following Poland–AOD sites: Strzyzow—Krzysztof Markowicz, Warsaw—Iwona Stachlewska, Sopot—Przemyslaw Makuch. Cimel sun-photometer calibrations were possible thanks to funding from the European Union's Horizon 2020 research and innovation programme under grant agreement No. 654109.

Conflicts of Interest: The authors declare no conflict of interest.

References

1. Brunekreef, B.; Holgate, S.T. Air pollution and health. *Lancet* **2002**, *360*, 1233–1242. [CrossRef]
2. Stocker, T.F.; Qin, D.; Plattner, G.-K.; Tignor, M.; Allen, S.K.; Boschung, J.; Nauels, A.; Xia, Y.; Bex, V.; Midgley, P.M. (Eds.) IPCC Summary for Policymakers. In *Climate Change 2013: The Physical Science Basis. Contribution of Working Group I to the Fifth Assessment Report of the Intergovernmental Panel on Climate Change*; Cambridge University Press: Cambridge, UK; New York, NY, USA, 2013.

3. Li, L.; Dubovik, O.; Derimian, Y.; Schuster, G.L.; Lapyonok, T.; Litvinov, P.; Ducos, F.; Fuertes, D.; Chen, C.; Li, Z.; et al. Retrieval of aerosol components directly from satellite and ground-based measurements. *Atmos. Chem. Phys. Discuss.* **2019**, *19*, 13409–13443. [CrossRef]
4. Li, J.; Li, X.; Carlson, B.E.; Kahn, R.A.; Lacis, A.A.; Dubovik, O.; Nakajima, T. Reducing multisensor monthly mean aerosol optical depth uncertainty: 2. Optimal locations for potential ground observation deployments. *J. Geophys. Res. Atmos.* **2017**, *122*, 3920–3928. [CrossRef]
5. Sogacheva, L.; Popp, T.; Sayer, A.M.; Dubovik, O.; Garay, M.J.; Heckel, A.; Hsu, N.C.; Jethva, H.; Kahn, R.A.; Kolmonen, P.; et al. Merging regional and global aerosol optical depth records from major available satellite products. *Atmos. Chem. Phys. Discuss.* **2020**, *20*, 2031–2056. [CrossRef]
6. Schutgens, N.; Sayer, A.M.; Heckel, A.; Hsu, C.; Jethva, H.; De Leeuw, G.; Leonard, P.J.T.; Levy, R.C.; Lipponen, A.; Lyapustin, A.; et al. An AeroCom–AeroSat study: Intercomparison of satellite AOD datasets for aerosol model evaluation. *Atmos. Chem. Phys. Discuss.* **2020**, *20*, 12431–12457. [CrossRef]
7. Lyapustin, A.; Wang, Y.; Xiong, X.; Meister, G.; Platnick, S.; Levy, R.; Franz, B.; Korkin, S.; Hilker, T.; Tucker, J.; et al. Scientific impact of MODIS C5 calibration degradation and C6+ improvements. *Atmos. Meas. Tech.* **2014**, *7*, 4353–4365. [CrossRef]
8. Eck, T.F.; Holben, B.N.; Reid, J.S.; Mukelabai, M.M.; Piketh, S.J.; Torres, O.; Jethva, H.T.; Hyer, E.J.; Ward, D.E.; Dubovik, O.; et al. A seasonal trend of single scattering albedo in southern African biomass-burning particles: Implications for satellite products and estimates of emissions for the world's largest biomass-burning source. *J. Geophys. Res. Atmos.* **2013**, *118*, 6414–6432. [CrossRef]
9. Chung, C.E. Aerosol Direct Radiative Forcing: A Review. In *Atmospheric Aerosols—Regional Characteristics—Chemistry and Physics*; Abdul-Razzak, H., Ed.; InTech: London, UK, 2012. [CrossRef]
10. Torres, O.; Bhartia, P.K.; Herman, J.R.; Ahmad, Z.; Gleason, J. Derivation of aerosol properties from satellite measurements of backscattered ultraviolet radiation: Theoretical basis. *J. Geophys. Res. Space Phys.* **1998**, *103*, 17099–17110. [CrossRef]
11. Torres, O.; Bhartia, P.K.; Sinyuk, A.; Welton, E.J.; Holben, B. Total Ozone Mapping Spectrometer measurements of aerosol absorption from space: Comparison to SAFARI 2000 ground-based observations. *J. Geophys. Res. Space Phys.* **2005**, *110*, 110. [CrossRef]
12. Hsu, N.C.; Lee, J.; Sayer, A.M.; Carletta, N.; Chen, S.-H.; Tucker, C.J.; Holben, B.N.; Tsay, S.-C. Retrieving near-global aerosol loading over land and ocean from AVHRR. *J. Geophys. Res. Atmos.* **2017**, *122*, 9968–9989. [CrossRef]
13. Sayer, A.M.; Hsu, N.C.; Lee, J.; Carletta, N.; Chen, S.-H.; Smirnov, A. Evaluation of NASA Deep Blue/SOAR aerosol retrieval algorithms applied to AVHRR measurements. *J. Geophys. Res. Atmos.* **2017**, *122*, 9945–9967. [CrossRef]
14. Sayer, A.M.; Hsu, N.C.; Bettenhausen, C.; Ahmad, Z.; Holben, B.N.; Smirnov, A.; Thomas, G.E.; Zhang, J. SeaWiFS Ocean Aerosol Retrieval (SOAR): Algorithm, validation, and comparison with other data sets. *J. Geophys. Res. Space Phys.* **2012**, *117*, 117. [CrossRef]
15. Hsu, N.C.; Tsay, S.-C.; King, M.D.; Herman, J.R. Aerosol Properties Over Bright-Reflecting Source Regions. *IEEE Trans. Geosci. Remote Sens.* **2004**, *42*, 557–569. [CrossRef]
16. Hsu, N.C.; Jeong, M.-J.; Bettenhausen, C.; Sayer, A.; Hansell, R.A.; Seftor, C.S.; Huang, J.; Tsay, S.-C. Enhanced Deep Blue aerosol retrieval algorithm: The second generation. *J. Geophys. Res. Atmos.* **2013**, *118*, 9296–9315. [CrossRef]
17. Levy, R.C.; Mattoo, S.; Munchak, L.A.; Remer, L.A.; Sayer, A.M.; Patadia, F.; Hsu, N.C. The Collection 6 MODIS aerosol products over land and ocean. *Atmos. Meas. Tech.* **2013**, *6*, 2989–3034. [CrossRef]
18. Gupta, P.; Levy, R.C.; Mattoo, S.; Remer, L.A.; Munchak, L.A. A surface reflectance scheme for retrieving aerosol optical depth over urban surfaces in MODIS Dark Target retrieval algorithm. *Atmos. Meas. Tech.* **2016**, *9*, 3293–3308. [CrossRef]
19. Gupta, P.; Remer, L.A.; Levy, R.C.; Mattoo, S. Validation of MODIS 3 km land aerosol optical depth from NASA's EOS Terra and Aqua missions. *Atmos. Meas. Tech.* **2018**, *11*, 3145–3159. [CrossRef]
20. Sayer, A.; Munchak, L.A.; Hsu, N.C.; Levy, R.C.; Bettenhausen, C.; Jeong, M.J. MODIS Collection 6 aerosol products: Comparison between Aqua's e-Deep Blue, Dark Target, and "merged" data sets, and usage recommendations. *J. Geophys. Res. Atmos.* **2014**, *119*, 13965–13989. [CrossRef]
21. Remer, L.A.; Mattoo, S.K.; Levy, R.C.; Munchak, L.A. MODIS 3 km aerosol product: Algorithm and global perspective. *Atmos. Meas. Tech.* **2013**, *6*, 1829–1844. [CrossRef]
22. Jethva, H.; Torres, O. Satellite-based evidence of wavelength-dependent aerosol absorption in biomass burning smoke inferred from Ozone Monitoring Instrument. *Atmos. Chem. Phys. Discuss.* **2011**, *11*, 10541–10551. [CrossRef]
23. Torres, O.; Tanskanen, A.; Veihelmann, B.; Ahn, C.; Braak, R.; Bhartia, P.K.; Veefkind, P.; Levelt, P.P. Aerosols and surface UV products from Ozone Monitoring Instrument observations: An overview. *J. Geophys. Res. Space Phys.* **2007**, *112*. [CrossRef]
24. Torres, O.; Ahn, C.; Chen, Z. Improvements to the OMI near-UV aerosol algorithm using A-train CALIOP and AIRS observations. *Atmos. Meas. Tech.* **2013**, *6*, 3257–3270. [CrossRef]
25. Torres, O.; Bhartia, P.K.; Jethva, H.; Ahn, C. Impact of the ozone monitoring instrument row anomaly on the long-term record of aerosol products. *Atmos. Meas. Tech.* **2018**, *11*, 2701–2715. [CrossRef]
26. Sayer, A.M.; Hsu, N.C.; Lee, J.; Kim, W.V.; Dutcher, S.T. Validation, Stability, and Consistency of MODIS Collection 6.1 and VIIRS Version 1 Deep Blue Aerosol Data Over Land. *J. Geophys. Res. Atmos.* **2019**, *124*, 4658–4688. [CrossRef]
27. Hsu, N.C.; Lee, J.; Sayer, A.M.; Kim, W.; Bettenhausen, C.; Tsay, S. VIIRS Deep Blue Aerosol Products Over Land: Extending the EOS Long-Term Aerosol Data Records. *J. Geophys. Res. Atmos.* **2019**, *124*, 4026–4053. [CrossRef]

28. Herman, M.; Deuzé, J.; Marchand, A.; Roger, B.; Lallart, P. Aerosol remote sensing from POLDER/ADEOS over the ocean: Improved retrieval using a nonspherical particle model. *J. Geophys. Res. Space Phys.* **2005**, *110*. [CrossRef]
29. Carboni, E.; Thomas, G.E.; Sayer, A.; Siddans, R.; Poulsen, C.A.; Grainger, R.G.; Ahn, C.; Antoine, D.J.; Bevan, S.; Braak, R.; et al. Intercomparison of desert dust optical depth from satellite measurements. *Atmos. Meas. Tech.* **2012**, *5*, 1973–2002. [CrossRef]
30. Yao, Z.; Li, J.; Han, H.-J.; Huang, A.; Sohn, B.J.; Zhang, P. Asian dust height and infrared optical depth retrievals over land from hyperspectral longwave infrared radiances. *J. Geophys. Res. Space Phys.* **2012**, *117*, 117. [CrossRef]
31. Yao, Z.; Li, J.; Zhao, Z.; Zhu, L.; Qi, J.; Che, H. Extracting Taklimakan Dust Parameters from AIRS with Artificial Neural Network Method. *Remote Sens.* **2019**, *11*, 2931. [CrossRef]
32. Capelle, V.; Chédin, A.; Pondrom, M.; Crevoisier, C.; Armante, R.; Crepeau, L.; Scott, N. Infrared dust aerosol optical depth retrieved daily from IASI and comparison with AERONET over the period 2007–2016. *Remote Sens. Environ.* **2018**, *206*, 15–32. [CrossRef]
33. De Leeuw, G.; Holzer-Popp, T.; Bevan, S.; Davies, W.H.; Descloitres, J.; Grainger, R.G.; Griesfeller, J.; Heckel, A.; Kinne, S.; Klüser, L.; et al. Evaluation of seven European aerosol optical depth retrieval algorithms for climate analysis. *Remote Sens. Environ.* **2015**, *162*, 295–315. [CrossRef]
34. Mei, L.; Rozanov, V.; Vountas, M.; Burrows, J.P.; Levy, R.C.; Lotz, W. Retrieval of aerosol optical properties using MERIS observations: Algorithm and some first results. *Remote Sens. Environ.* **2017**, *197*, 125–140. [CrossRef]
35. Mei, L.; Rozanov, V.; Vountas, M.; Burrows, J.P.; Richter, A. XBAER-derived aerosol optical thickness from OLCI/Sentinel-3 observation. *Atmos. Chem. Phys. Discuss.* **2018**, *18*, 2511–2523. [CrossRef]
36. Kolmonen, P.; Sogacheva, L.; Virtanen, T.H.; De Leeuw, G.; Kulmala, M. The ADV/ASV AATSR aerosol retrieval algorithm: Current status and presentation of a full-mission AOD dataset. *Int. J. Digit. Earth* **2015**, *9*, 545–561. [CrossRef]
37. Che, Y.; Mei, L.; Xue, Y.; Guang, J.; She, L.; Li, Y.; Heckel, A.; North, P. Validation of Aerosol Products from AATSR and MERIS/AATSR Synergy Algorithms—Part 1: Global Evaluation. *Remote Sens.* **2018**, *10*, 1414. [CrossRef]
38. Henocq, C.; North, P.; Heckel, A.; Ferron, S.; Lamquin, N.; Dransfeld, S.; Bourg, L.; Tote, C.; Ramon, D. OLCI/SLSTR SYN L2 Algorithm and Products Overview. *Int. Geosci. Remote Sens. Sympos. (IGARSS)* **2018**, 8723–8726. [CrossRef]
39. EUMETSAT. Available online: https://www.eumetsat.int/S3-AOD (accessed on 7 February 2021).
40. Martonchik, J.V.; Kahn, R.A.; Diner, D.J. Retrieval of aerosol properties over land using MISR observations. In *Satellite Aerosol Remote Sensing Over Land*; Kokhanovsky, A.A., de Leeuw, G., Eds.; Springer: Berlin/Heidelberg, Germany, 2009; pp. 267–293.
41. Kahn, R.A.; Gaitley, B.J.; Garay, M.J.; Diner, D.J.; Eck, T.F.; Smirnov, A.; Holben, B.N. Multiangle Imaging SpectroRadiometer global aerosol product assessment by comparison with the Aerosol Robotic Network. *J. Geophys. Res. Space Phys.* **2010**, *115*, 115. [CrossRef]
42. Garay, M.J.; Kalashnikova, O.V.; Bull, M.A. Development and assessment of a higher-spatial-resolution (4.4 km) MISR aerosol optical depth product using AERONET-DRAGON data. *Atmos. Chem. Phys. Discuss.* **2017**, *17*, 5095–5106. [CrossRef]
43. Garay, M.J.; Witek, M.L.; Kahn, R.A.; Seidel, F.C.; Limbacher, J.A.; Bull, M.A.; Diner, D.J.; Hansen, E.G.; Kalashnikova, O.V.; Lee, H.; et al. Introducing the 4.4 km spatial resolution Multi-Angle Imaging SpectroRadiometer (MISR) aerosol product. *Atmos. Meas. Tech.* **2020**, *13*, 593–628. [CrossRef]
44. Holzer-Popp, T.; Schroedter-Homscheidt, M.; Breitkreuz, H.; Martynenko, D.; Klüser, L. Improvements of synergetic aerosol retrieval for ENVISAT. *Atmos. Chem. Phys. Discuss.* **2008**, *8*, 7651–7672. [CrossRef]
45. Von Hoyningen-Huene, W.; Kokhanovsky, A.A.; Wuttke, M.W.; Buchwitz, M.; Noël, S.; Gerilowski, K.; Burrows, J.P.; Latter, B.; Siddans, R.; Kerridge, B.J. Validation of SCIAMACHY top-of-atmosphere reflectance for aerosol remote sensing using MERIS L1 data. *Atmos. Chem. Phys. Discuss.* **2007**, *7*, 97–106. [CrossRef]
46. Rault, D.F.; Loughman, R.P. The OMPS Limb Profiler Environmental Data Record Algorithm Theoretical Basis Document and Expected Performance. *IEEE Trans. Geosci. Remote Sens.* **2012**, *51*, 2505–2527. [CrossRef]
47. Loughman, R.; Bhartia, P.K.; Chen, Z.; Xu, P.; Nyaku, E.; Taha, G. The Ozone Mapping and Profiler Suite (OMPS) Limb Profiler (LP) Version 1 aerosol extinction retrieval algorithm: Theoretical basis. *Atmos. Meas. Tech.* **2018**, *11*, 2633–2651. [CrossRef]
48. Thomason, L.W.; Burton, S.P.; Luo, B.-P.; Peter, T. SAGE II measurements of stratospheric aerosol properties at non-volcanic levels. *Atmos. Chem. Phys. Discuss.* **2008**, *8*, 983–995. [CrossRef]
49. Rieger, L.A.; Bourassa, A.E.; Degenstein, D.A. Merging the OSIRIS and SAGE II stratospheric aerosol records. *J. Geophys. Res. Atmos.* **2015**, *120*, 8890–8904. [CrossRef]
50. Rieger, L.A.; Malinina, E.P.; Rozanov, A.V.; Burrows, J.P.; Bourassa, A.E.; Degenstein, D.A. A study of the approaches used to retrieve aerosol extinction, as applied to limb observations made by OSIRIS and SCIAMACHY. *Atmos. Meas. Tech.* **2018**, *11*, 3433–3445. [CrossRef]
51. Omar, A.H.; Winker, D.M.; Tackett, J.L.; Giles, D.M.; Kar, J.; Liu, Z.; Vaughan, M.A.; Powell, K.A.; Trepte, C.R. CALIOP and AERONET aerosol optical depth comparisons: One size fits none. *J. Geophys. Res. Atmos.* **2013**, *118*, 4748–4766. [CrossRef]
52. Young, S.A.; Vaughan, M.A.; Garnier, A.; Tackett, J.L.; Lambeth, J.D.; Powell, K.A. Extinction and optical depth retrievals for CALIPSO's Version 4 data release. *Atmos. Meas. Tech.* **2018**, *11*, 5701–5727. [CrossRef]
53. Knapp, K.R.; Frouin, R.; Kondragunta, S.; Prados, A. Toward aerosol optical depth retrievals over land from GOES visible radiances: Determining surface reflectance. *Int. J. Remote Sens.* **2005**, *26*, 4097–4116. [CrossRef]
54. Zhang, H.; Hoff, R.M.; Kondragunta, S.; Laszlo, I.; Lyapustin, A. Aerosol optical depth (AOD) retrieval using simultaneous GOES-East and GOES-West reflected radiances over the western United States. *Atmos. Meas. Tech.* **2013**, *6*, 471–486. [CrossRef]

55. Greenwald, T.J.; Pierce, R.B.; Schaack, T.K.; Otkin, J.A.; Rogal, M.; Bah, K.; Lenzen, A.J.; Nelson, J.P.; Li, J.; Huang, H.-L. Real-Time Simulation of the GOES-R ABI for User Readiness and Product Evaluation. *Bull. Am. Meteorol. Soc.* **2016**, *97*, 245–261. [CrossRef]
56. Bernard, E.; Moulin, C.; Ramon, D.; Jolivet, D.; Riedi, J.; Nicolas, J.-M. Description and validation of an AOT product over land at the 0.6 µm channel of the SEVIRI sensor onboard MSG. *Atmos. Meas. Tech.* **2011**, *4*, 2543–2565. [CrossRef]
57. Zawadzka, O.; Markowicz, K. Retrieval of Aerosol Optical Depth from Optimal Interpolation Approach Applied to SEVIRI Data. *Remote Sens.* **2014**, *6*, 7182–7211. [CrossRef]
58. Zawadzka-Manko, O.; Stachlewska, I.S.; Markowicz, K.M. Near-Real-Time Application of SEVIRI Aerosol Optical Depth Algorithm. *Remote Sens.* **2020**, *12*, 1481. [CrossRef]
59. Popp, C.; Hauser, A.; Foppa, N.; Wunderle, S. Remote sensing of aerosol optical depth over central Europe from MSG-SEVIRI data and accuracy assessment with ground-based AERONET measurements. *J. Geophys. Res. Space Phys.* **2007**, *112*. [CrossRef]
60. Lim, H.; Choi, M.; Kim, J.; Kasai, Y.; Chan, P.W. AHI/Himawari-8 Yonsei Aerosol Retrieval (YAER): Algorithm, Validation and Merged Products. *Remote Sens.* **2018**, *10*, 699. [CrossRef]
61. Zhang, W.; Xu, H.; Zheng, F. Aerosol Optical Depth Retrieval over East Asia Using Himawari-8/AHI Data. *Remote Sens.* **2018**, *10*, 137. [CrossRef]
62. Yang, F.; Wang, Y.; Tao, J.; Wang, Z.; Fan, M.; De Leeuw, G.; Chen, L. Preliminary Investigation of a New AHI Aerosol Optical Depth (AOD) Retrieval Algorithm and Evaluation with Multiple Source AOD Measurements in China. *Remote Sens.* **2018**, *10*, 748. [CrossRef]
63. Sayer, A.M.; Govaerts, Y.; Kolmonen, P.; Lipponen, A.; Luffarelli, M.; Mielonen, T.; Patadia, F.; Popp, T.; Povey, A.C.; Stebel, K.; et al. A review and framework for the evaluation of pixel-level uncertainty estimates in satellite aerosol remote sensing. *Atmos. Meas. Tech.* **2020**, *13*, 373–404. [CrossRef]
64. Wei, X.; Chang, N.-B.; Bai, K.; Gao, W. Satellite remote sensing of aerosol optical depth: Advances, challenges, and perspectives. *Crit. Rev. Environ. Sci. Technol.* **2019**, *50*, 1640–1725. [CrossRef]
65. Palacios-Peña, L.; Baró, R.; Baklanov, A.; Balzarini, A.; Brunner, D.; Forkel, R.; Hirtl, M.; Honzak, L.; López-Romero, J.M.; Montávez, J.P.; et al. An assessment of aerosol optical properties from remote-sensing observations and regional chemistry–climate coupled models over Europe. *Atmos. Chem. Phys. Discuss.* **2018**, *18*, 5021–5043. [CrossRef]
66. Kokhanovsky, A.; Breon, F.-M.; Cacciari, A.; Carboni, E.; Diner, D.; Di Nicolantonio, W.; Grainger, R.; Grey, W.; Höller, R.; Lee, K.-H.; et al. Aerosol remote sensing over land: A comparison of satellite retrievals using different algorithms and instruments. *Atmos. Res.* **2007**, *85*, 372–394. [CrossRef]
67. Li, Z.; Zhao, X.; Kahn, R.; Mishchenko, M.; Remer, L.; Lee, K.-H.; Wang, M.; Laszlo, I.; Nakajima, T.; Maring, H. Uncertainties in satellite remote sensing of aerosols and impact on monitoring its long-term trend: A review and perspective. *Ann. Geophys.* **2009**, *27*, 2755–2770. [CrossRef]
68. Sogacheva, L.; Kolmonen, P.; Virtanen, T.H.; Rodriguez, E.; Saponaro, G.; De Leeuw, G. Post-processing to remove residual clouds from aerosol optical depth retrieved using the Advanced Along Track Scanning Radiometer. *Atmos. Meas. Tech.* **2017**, *10*, 491–505. [CrossRef]
69. Ignatov, A. Estimation of the aerosol phase function in backscatter from simultaneous satellite and sun-photometer meas-urements. *J. Appl. Meteorol. Climatol.* **1997**, *36*, 688–694. [CrossRef]
70. Tang, J.; Xue, Y.; Yu, T.; Guan, Y. Aerosol optical thickness determination by exploiting the synergy of TERRA and AQUA MODIS. *Remote Sens. Environ.* **2005**, *94*, 327–334. [CrossRef]
71. Kinne, S. Remote sensing data combinations: Superior global maps for aerosol optical depth. In *Satellite Aerosol Remote Sensing over Land*; Springer: Berlin/Heidelberg, Germany, 2009; pp. 361–381. [CrossRef]
72. Kinne, S.; O'Donnel, D.; Stier, P.; Kloster, S.; Zhang, K.; Schmidt, H.; Rast, S.; Giorgetta, M.A.; Eck, T.F.; Stevens, B. MAC-v1: A new global aerosol climatology for climate studies. *J. Adv. Model. Earth Syst.* **2013**, *5*, 704–740. [CrossRef]
73. Bréon, F.-M.; Vermeulen, A.; Descloitres, J. An evaluation of satellite aerosol products against sunphotometer measurements. *Remote Sens. Environ.* **2011**, *115*, 3102–3111. [CrossRef]
74. Petrenko, M.; Ichoku, C. Coherent uncertainty analysis of aerosol measurements from multiple satellite sensors. *Atmos. Chem. Phys. Discuss.* **2013**, *13*, 6777–6805. [CrossRef]
75. Holben, B.N.; Tanré, D.; Smirnov, A.; Eck, T.F.; Slutsker, I.; Abuhassan, N.; Newcomb, W.W.; Schafer, J.S.; Chatenet, B.; Lavenu, F.; et al. An emerging ground-based aerosol climatology: Aerosol optical depth from AERONET. *J. Geophys. Res. Space Phys.* **2001**, *106*, 12067–12097. [CrossRef]
76. Sowden, M.; Mueller, U.; Blake, D. Review of surface particulate monitoring of dust events using geostationary satellite remote sensing. *Atmos. Environ.* **2018**, *183*, 154–164. [CrossRef]
77. Govaerts, Y.M.; Wagner, S.; Lattanzio, A.; Watts, P. Joint retrieval of surface reflectance and aerosol optical depth from MSG/SEVIRI observations with an optimal estimation approach: 1. Theory. *J. Geophys. Res. Space Phys.* **2010**, *115*, 02203. [CrossRef]
78. Jolivet, D.; Ramon, D.; Riedi, J.; Roebeling, R. Aerosol Retrievals from METEOSAT-8. SAF on Climate Monitoring, Visiting Scientist Report 2006. Available online: https://www.knmi.nl/kennis-en-datacentrum/publicatie/aerosol-retrievals-from-meteosat-8 (accessed on 2 February 2021).
79. Carrer, D.; Roujean, J.-L.; Hautecoeur, O.; Elias, T. Daily estimates of aerosol optical thickness over land surface based on a directional and temporal analysis of SEVIRI MSG visible observations. *J. Geophys. Res. Space Phys.* **2010**, *115*, 10208. [CrossRef]

80. Bulgin, C.E.; Palmer, P.I.; Merchant, C.J.; Siddans, R.; Gonzi, S.; Poulsen, C.A.; Thomas, G.E.; Sayer, A.M.; Carboni, E.; Grainger, R.G.; et al. Quantifying the response of the ORAC aerosol optical depth retrieval for MSG SEVIRI to aerosol model assumptions. *J. Geophys. Res. Space Phys.* **2011**, *116*. [CrossRef]
81. Mei, L.; Xue, Y.; De Leeuw, G.; Holzer-Popp, T.; Guang, J.; Li, Y.; Yang, L.; Xu, H.; Xu, X.; Li, C.; et al. Retrieval of aerosol optical depth over land based on a time series technique using MSG/SEVIRI data. *Atmos. Chem. Phys. Discuss.* **2012**, *12*, 9167–9185. [CrossRef]
82. Fernandes, A.P.; Riffler, M.; Ferreira, J.; Wunderle, S.; Borrego, C.; Tchepeld, O. Comparisons of aerosol optical depth provided by SEVIRI satellite observations and CAMx air quality modelling. In Proceedings of the 36th International Symposium on Remote Sensing of Environment, Berlin, Germany, 11–15 May 2015; Schreier, G., Skrovseth, P.E., Staudenrausch, H., Eds.; Copernicus Gesellschaft Mbh: Gottingen, Germany, 2015; pp. 187–193.
83. Clerbaux, N.; Ipe, A.; De Bock, V.; Urbain, M.; Baudrez, E.; Velazquez-Blazquez, A.; Akkermans, T.; Moreels, J.; Hollmann, R.; Selbach, N.; et al. CM SAF Aerosol Optical Depth (AOD) Data Record–Edition 1. *Satell. Appl. Facil. Clim. Monit.* **2017**. [CrossRef]
84. Stebel, K.; Stachlewska, I.S.; Nemuc, A.; Horálek, J.; Schneider, P.; Ajtai, N.; Diamandi, A.; Benešova, N.; Boldeanu, M.; Botezan, C.; et al. SAMIRA—SAtellite based Monitoring Initiative for Regional Air quality. *Remote Sens.* **2021**, submitted.
85. Aminou, D.M.A. *MSG's SEVIRI Instrument, ESA Bulletin. Bulletin ASE*; European Space Agency: Paris, France, 2002; Volume 111.
86. Riedi, J.; Nicolas, J.M. *Science_modules_msg.c*; Laboratoire d'Optique Atmospherique: Lille, France, 2005.
87. Rodgers, C.D. *Inverse Methods for Atmospheric Sounding: Theory and Practice*; World Scientific: Singapore, 2002.
88. Levy, R.C.; Remer, L.; Tanré, D.; Mattoo, S.; Kaufman, Y.J. Algorithm for Remote Sensing of Tropospheric Aerosol over Dark Targets from MODIS: Collections 005 and 051: Revision 2; February 2009. MODIS Algorithm Theoretical Basis Document; 2009. Available online: https://atmosphere-imager.gsfc.nasa.gov/sites/default/files/ModAtmo/ATBD_MOD04_C005_rev2_0.pdf (accessed on 28 September 2020).
89. Kaufman, Y.J.; Wald, A.E.; Remer, L.A.; Gao, B.C.; Li, R.-R.; Flynn, L. The MODIS 2.1-/spl mu/m channel-correlation with visible reflectance for use in remote sensing of aerosol. *IEEE Trans. Geosci. Remote Sens.* **1997**, *35*, 1286–1298. [CrossRef]
90. Tanré, D.; Kaufman, Y.J.; Herman, M.; Mattoo, S. Remote sensing of aerosol properties over oceans using the MODIS/EOS spectral radiances. *J. Geophys. Res. Space Phys.* **1997**, *102*, 16971–16988. [CrossRef]
91. Levy, R.C.; Remer, L.A.; Martins, J.V.; Kaufman, Y.J.; Plana-Fattori, A.; Redemann, J.; Wenny, B. Evaluation of the MODIS Aerosol Retrievals over Ocean and Land during CLAMS. *J. Atmos. Sci.* **2005**, *62*, 974–992. [CrossRef]
92. Levy, R.C.; Remer, L.A.; Mattoo, S.; Vermote, E.F.; Kaufman, Y.J. Second-generation operational algorithm: Retrieval of aerosol properties over land from inversion of Moderate Resolution Imaging Spectroradiometer spectral reflectance. *J. Geophys. Res. Space Phys.* **2007**, *112*. [CrossRef]
93. Levy, R.C.; Remer, L.A.; Kleidman, R.; Mattoo, S.K.; Ichoku, C.; Kahn, R.A.; Eck, T.F. Global evaluation of the Collection 5 MODIS dark-target aerosol products over land. *Atmos. Chem. Phys. Discuss.* **2010**, *10*, 10399–10420. [CrossRef]
94. Remer, L.A.; Kaufman, Y.J.; Tanré, D.; Mattoo, S.; Chu, D.A.; Martins, J.V.; Li, R.R.; Ichoku, C.; Levy, R.C.; Kleidman, R.G.; et al. The MODIS Aerosol Algorithm, Products, and Validation. *J. Atmos. Sci.* **2005**, *62*, 947–973. [CrossRef]
95. Remer, L.A.; Kleidman, R.G.; Levy, R.C.; Kaufman, Y.J.; Tanré, D.; Mattoo, S.; Martins, J.V.; Ichoku, C.; Koren, I.; Yu, H.; et al. Global aerosol climatology from the MODIS satellite sensors. *J. Geophys. Res. Space Phys.* **2008**, *113*, 14. [CrossRef]
96. Levy, R.C.; Munchak, L.A.; Mattoo, S.K.; Patadia, F.; Remer, L.A.; Holz, R.E. Towards a long-term global aerosol optical depth record: Applying a consistent aerosol retrieval algorithm to MODIS and VIIRS-observed reflectance. *Atmos. Meas. Tech.* **2015**, *8*, 4083–4110. [CrossRef]
97. Wang, D.; Szczepanik, D.; Stachlewska, I.S. Interrelations between surface, boundary layer, and columnar aerosol properties derived in summer and early autumn over a continental urban site in Warsaw, Poland. *Atmos. Chem. Phys. Discuss.* **2019**, *19*, 13097–13128. [CrossRef]
98. Popp, T.; De Leeuw, G.; Bingen, C.; Brühl, C.; Capelle, V.; Chedin, A.; Clarisse, L.; Dubovik, O.; Grainger, R.; Griesfeller, J.; et al. Development, Production and Evaluation of Aerosol Climate Data Records from European Satellite Observations (Aerosol_cci). *Remote Sens.* **2016**, *8*, 421. [CrossRef]
99. Schutgens, N.A.J. Site representativity of AERONET and GAW remotely sensed aerosol optical thickness and absorbing aerosol optical thickness observations. *Atmos. Chem. Phys. Discuss.* **2020**, *20*, 7473–7488. [CrossRef]
100. Szczepanik, D.; Markowicz, K. The relation between columnar and surface aerosol optical properties in a background environment. *Atmos. Pollut. Res.* **2018**, *9*, 246–256. [CrossRef]
101. Sun, W.; Videen, G.; Kato, S.; Lin, B.; Lukashin, C.; Hu, Y. A study of subvisual clouds and their radiation effect with a synergy of CERES, MODIS, CALIPSO, and AIRS data. *J. Geophys. Res. Space Phys.* **2011**, *116*. [CrossRef]
102. Huang, J.; Hsu, N.C.; Tsay, S.-C.; Jeong, M.-J.; Holben, B.N.; Berkoff, T.A.; Welton, E.J. Susceptibility of aerosol optical thickness retrievals to thin cirrus contamination during the BASE-ASIA campaign. *J. Geophys. Res. Space Phys.* **2011**, *116*. [CrossRef]
103. Wollner, U.; Koren, I.; Altaratz, O.; Remer, L.A. On the signature of the cirrus twilight zone. *Environ. Res. Lett.* **2014**, *9*, 094010. [CrossRef]
104. Riuttanen, L.; Bister, M.; Kerminen, V.-M.; John, V.O.; Sundström, A.-M.; Maso, M.D.; Räisänen, J.; Sinclair, V.A.; Makkonen, R.; Xausa, F.; et al. Observational evidence for aerosols increasing upper tropospheric humidity. *Atmos. Chem. Phys. Discuss.* **2016**, *16*, 14331–14342. [CrossRef]

105. Spencer, R.S.; Levy, R.C.; Remer, L.A.; Mattoo, S.; Arnold, G.T.; Hlavka, D.L.; Meyer, K.G.; Marshak, A.; Wilcox, E.M.; Platnick, S.E. Exploring Aerosols Near Clouds with High-Spatial-Resolution Aircraft Remote Sensing During SEAC 4 RS. *J. Geophys. Res. Atmos.* **2019**, *124*, 2148–2173. [CrossRef] [PubMed]
106. Koepke, P.; Hess, M.; Schult, I.; Shettle, E.P. *Global Aerosol Data Set; Report No. 243*; Max-Planck-Institut für Meteorologie: Hamburg, Germany, 1997.